Cell Reports

Article

Tace/ADAM17 is a bi-directional regulator of axon guidance that coordinates distinct Frazzled and Dcc receptor signaling outputs

Graphical abstract

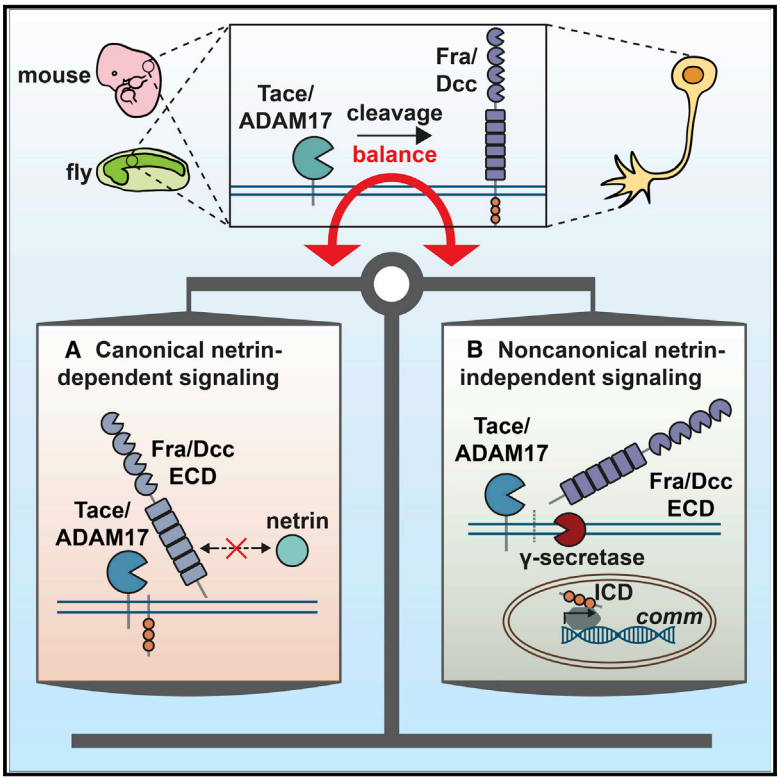

Authors

Yixin Zang, Karina Chaudhari, Greg J. Bashaw

Correspondence

gbashaw@pennmedicine.upenn.edu

In brief

The Fra/Dcc axon guidance receptor produces multiple signaling outputs, yet how neurons coordinate these pathways to make correct guidance decisions is unclear. Zang et al. demonstrate that Tace and its vertebrate homolog ADAM17 regulate commissural axon guidance during development by establishing a balance between distinct Fra/Dcc receptor signaling activities.

Highlights

- Tace/ADAM17 regulates commissural axon guidance during neuronal development
- Fra and Dcc receptors are substrates for Tace/ADAM17
- Tace/ADAM17 control receptor signaling by coordinating distinct signaling outputs
- The function of Tace and ADAM17 in neurodevelopment is evolutionarily conserved

Zang et al., 2022, Cell Reports *41*, 111785
December 6, 2022
https://doi.org/10.1016/j.celrep.2022.111785

CellPress

Cell Reports

CellPress
OPEN ACCESS

Article

Tace/ADAM17 is a bi-directional regulator of axon guidance that coordinates distinct Frazzled and Dcc receptor signaling outputs

Yixin Zang,[1] Karina Chaudhari,[1,2] and Greg J. Bashaw[1,3,*]
[1]Department of Neuroscience, Perelman School of Medicine, University of Pennsylvania, Philadelphia, PA 19104, USA
[2]Present address: The Solomon H. Snyder Department of Neuroscience, Johns Hopkins University School of Medicine, Baltimore, MD 21205, USA
[3]Lead contact
*Correspondence: gbashaw@pennmedicine.upenn.edu
https://doi.org/10.1016/j.celrep.2022.111785

SUMMARY

Frazzled (Fra) and deleted in colorectal cancer (Dcc) are homologous receptors that promote axon attraction in response to netrin. In *Drosophila*, Fra also acts independently of netrin by releasing an intracellular domain (ICD) that activates gene transcription. How neurons coordinate these pathways to make accurate guidance decisions is unclear. Here we show that the ADAM metalloprotease Tace cleaves Fra, and this instructs the switch between the two pathways. Genetic manipulations that either increase or decrease Tace levels disrupt midline crossing of commissural axons. These conflicting phenotypes reflect Tace's function as a bi-directional regulator of axon guidance, a function conserved in its vertebrate homolog ADAM17: while Tace induces the formation of the Fra ICD to activate transcription, excessive Tace cleavage of Fra and Dcc suppresses the response to netrin. We propose that Tace and ADAM17 are key regulators of midline axon guidance by establishing the balance between netrin-dependent and netrin-independent signaling.

INTRODUCTION

Establishing neuronal circuits requires accurate guidance and targeting of axons during development. This highly regulated process relies on a conserved group of transmembrane axon guidance receptors, which transmit information across the growth cone plasma membrane at the tip of the navigating axon. As growth cones explore the extracellular environment, axon guidance receptors respond to guidance cues, triggering downstream signaling cascades to either attract or repel axons. Attractive and repulsive forces are precisely balanced to ensure appropriate pathfinding at multiple choice points along the axonal trajectory. One of the most important choice points is the midline of the body.[1,2] Axon commissures that cross the midline and bridge the two sides of the central nervous system (CNS) are essential for the proper coordination of motor, sensory, and cognitive functions. Aberrant commissure formation is associated with movement disorders and other neurological deficits in humans.[3–5] Indeed, mutant alleles of several axon guidance receptors are causatively linked to congenital mirror movement disorder,[6,7] horizontal gaze palsy with progressive scoliosis,[8] dyslexia,[9] and intellectual disabilities.[10]

The ventral midline of the developing spinal cord and the analogous *Drosophila* ventral nerve cord serve as important model systems to study commissural axon guidance. In both systems, specialized cells at the midline secrete conserved cues that guide commissural axons across the midline. This process requires the function of the conserved axon guidance receptor Frazzled (Fra) and its vertebrate homolog, deleted in colorectal cancer (Dcc).[11–19] Upon stimulation by their ligand, netrin, Fra and Dcc promote axon growth and attraction by recruiting downstream signaling effectors to orchestrate local cytoskeletal remodeling.[20] In addition, Fra also functions independent of netrin in *Drosophila* in a "non-canonical" pathway. In commissural neurons whose axons are actively crossing the midline, Fra undergoes intramembrane cleavage by the γ-secretase complex to generate intracellular domains (ICDs).[1,21] The released ICDs can translocate to the nucleus to activate the transcription of *commissureless* (*comm*), which encodes an endosomal sorting protein that prevents the repulsive response to Slit and is essential for midline crossing.[1,22,23] Evidence in cancer cell lines indicates that Fra's vertebrate homologs, Dcc and neogenin, are also cleaved by γ-secretase to generate ICDs that can enter the nucleus and regulate transcription,[24,25] raising the intriguing possibility that a similar non-canonical pathway might function in commissural axon guidance in vertebrates. However, since Fra's transcriptional activity does not require netrin, it remains unclear what signal activates γ-secretase to cleave Fra and whether the same mechanism is conserved for Dcc.

The complex network of signaling events downstream of Fra/Dcc presents the neuron with the challenging task of selecting and coordinating among different receptor signaling outputs. In

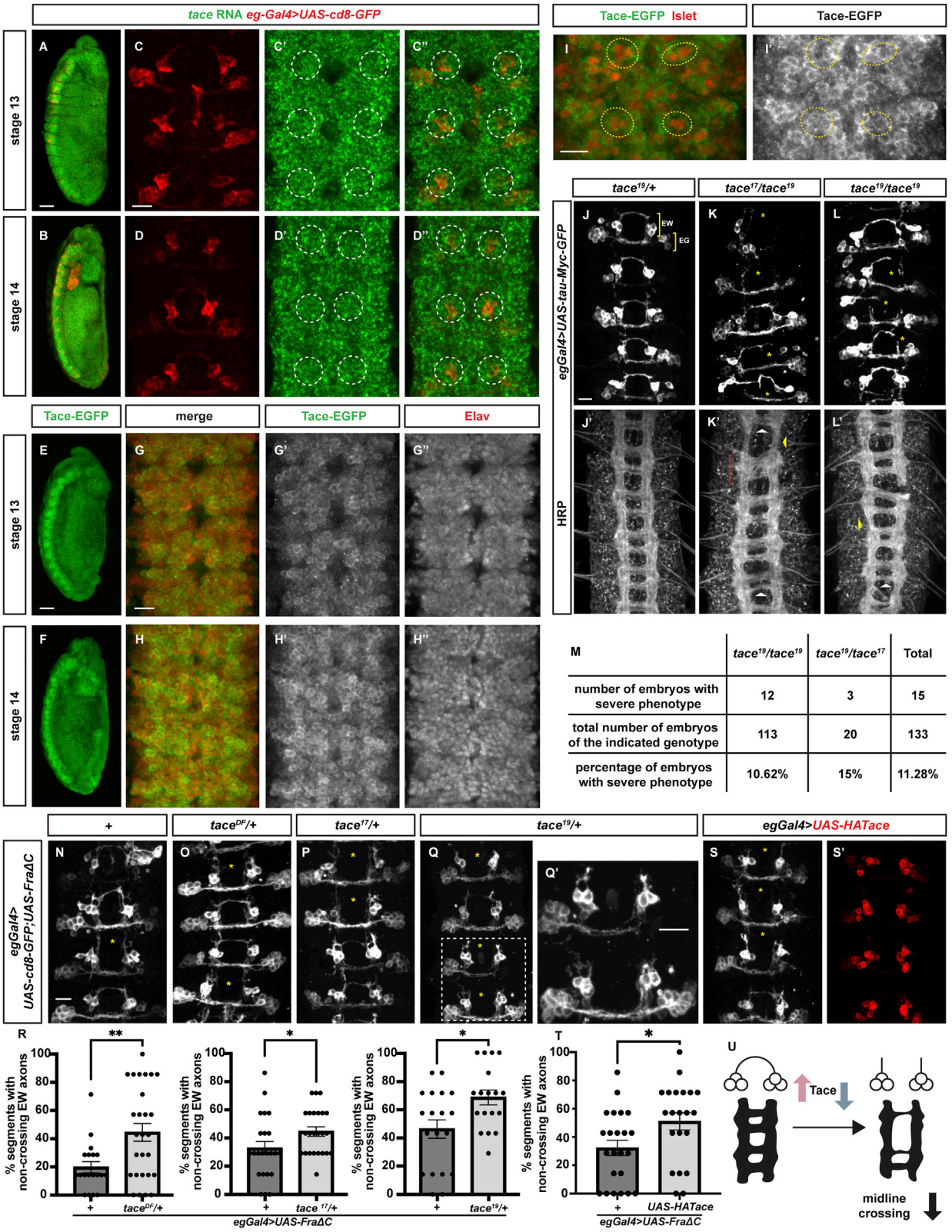

(legend on next page)

particular, at the time of crossing, commissural axons need to activate both the canonical netrin-dependent pathway and the non-canonical netrin-independent pathway, to initiate attraction and to inhibit repulsion, respectively. However, little is known about the mechanisms that activate and coordinate these pathways. Proteolytic processing has emerged as a critical mechanism for regulating the function of transmembrane receptors.[26–28] In particular, the ADAM (a disintegrin and metalloprotease) family of transmembrane proteases cleaves the extracellular juxtamembrane region of transmembrane proteins to release their extracellular domains (ECDs).[29,30] Nearly 30 members of the ADAM family have been identified in mice and humans, with many playing key roles in neurodevelopment.[31] Importantly, inhibiting ADAM activity with broad-spectrum ADAM inhibitors potentiates netrin responses in rat dorsal spinal cord explants.[32] This result suggests that ADAM proteases likely regulate netrin responses by modulating the function of Dcc, yet the identity of the ADAM, the precise mechanism, and the physiological significance of this proteolysis are unknown.

Here we establish a conserved and essential role for Tace and ADAM17 in cleaving Fra and Dcc and demonstrate that this proteolysis bi-directionally regulates axon guidance at the midline. Tace shows striking enrichment in the embryonic nerve cord of *Drosophila.* Unexpectedly, both *tace* mutants and Tace overexpression lead to deficits in midline axon guidance. To dissect the mechanism behind these conflicting phenotypes, we provide genetic and biochemical evidence indicating that Tace can regulate both the canonical and the non-canonical pathway. While Tace activates the non-canonical pathway by initiating ICD formation and regulating the transcription of *comm*, Tace also inhibits the canonical pathway by reducing commissural axon's responsiveness to netrin. Importantly, phenotypes in the embryonic mouse spinal cord closely mirror those seen in *Drosophila*, strongly suggesting that the function of Tace is evolutionarily conserved in vertebrates. In summary, our data highlight a previously uncharacterized mode of action for ADAMs, whereby they function as bi-directional regulators of transmembrane receptors to coordinate and balance different signaling outputs.

RESULTS

Tace is expressed in the developing *Drosophila* ventral nerve cord

To characterize the expression pattern of Tace, we performed fluorescent RNA *in situ* hybridization (RNA FISH) on *Drosophila* embryos (Figures 1A–1D″). *tace* transcripts are maternally deposited, as the *tace* RNA FISH signal is detected before the onset of zygotic transcription (Figure S1A). Despite this, we observe a marked decrease in expression in *tace* mutant embryos compared with sibling controls, confirming the specificity of the *tace in situ* probe (Figures S1B–S1E′). At crossing stages (stages 13 and 14), *tace* mRNA is broadly expressed, but is especially enriched in the ventral nerve cord (Figures 1A and 1B). We next examined Tace expression in a subset of commissural neurons, the eagle neurons, labeled with a membrane-targeted GFP (*UAS-cd8-GFP*; Figures 1C and 1D). Puncta of *tace* mRNA colocalize with the cell bodies of eagle neurons (Figures 1C″ and 1D″). To visualize the cellular and subcellular localization of Tace protein, we generated an endogenously GFP-tagged Tace-EGFP line. Tace protein expression begins from approximately stage 13 and persists throughout development (Figures 1E, 1F, S1F, and S1G). Like Tace mRNA, Tace protein is broadly expressed and is highly enriched in the brain and ventral nerve cord. Further, using Elav, a marker for differentiated neurons, we observe that Tace is expressed in most neurons (Figures 1G–1H″ and S1H–S1I″). Colabeling with the Islet transcription factor shows that Tace is expressed in eagle commissural interneurons (Figures 1I and 1I′).[33] Tace is also expressed in a small subset of Reversed polarity (Repo)-positive glia (Figures S1J–S1L′), but is not expressed in midline glia (Figures S1M–S1N″). Interestingly, across all developmental stages, Tace protein is exclusively detected in the soma but not in the axons (Figures S1O–S1Q″), suggesting potential somatic functions of Tace as opposed to axonal roles.

tace is required for midline crossing

To study the function of *tace* in commissural axon guidance, we used CRISPR-Cas9 to generate two independent *tace*-null

Figure 1. Tace is expressed in the *Drosophila* ventral nerve cord and functions in commissural axon guidance

(A–I) Tace RNA and protein expression in stage 13 and 14 embryos.

(A–D″) RNA FISH for *tace*, labeled in green, and eagle neurons labeled in red. *tace* transcripts are enriched in the CNS and are expressed in eagle neurons (dotted white circles).

(E–H″) Tace protein expression is detected in the brain and the ventral nerve cord by the endogenous GFP tag (green) and colocalizes with a large subset of the neurons, labeled by Elav (red).

(I and I′) Tace protein colocalizes with the Islet-positive (red) EW neurons (yellow dotted circles).

(J–R) *tace* mutant phenotypes in stage 15–16 embryos. GFP labels the EW and EG population of eagle neurons (yellow brackets in J).

(K and L) Midline crossing of EW axons is disrupted in *tace* mutant embryos (asterisks indicate non-crossing segments).

(K′ and L′) HRP-positive axon scaffolds show thinning of commissures (white triangles) and longitudinal tracks (yellow triangles). Red bracket indicates the rare occurrence of a segment with thickened commissures.

(M) Summary of embryos analyzed.

(N–Q′) *tace* mutants significantly enhance non-crossing defects in embryos that express FraΔC (indicated by asterisks). The region outlined in Q is magnified in Q′.

(R) For embryos with indicated *tace* alleles, the percentage of non-crossing segments was compared with the corresponding FraΔC-overexpressing control group and quantified by Student's t test. Number of embryos, n = 19, 27, 23, 24, 19, 18.

(S and T) Compared with the control group, Tace overexpression significantly enhances the EW non-crossing phenotype (indicated by asterisks), which was quantified by Student's t test in (T). Number of embryos, n = 23, 21.

(U) Schematic describing the phenotypes observed in *tace* loss and gain of function.

Scale bars represent 40 μm in (A), (B), (E), and (F) and 10 μm in the rest of the images. Anterior is up. Error bars indicate SEM; *p < 0.0332, **p < 0.0021.

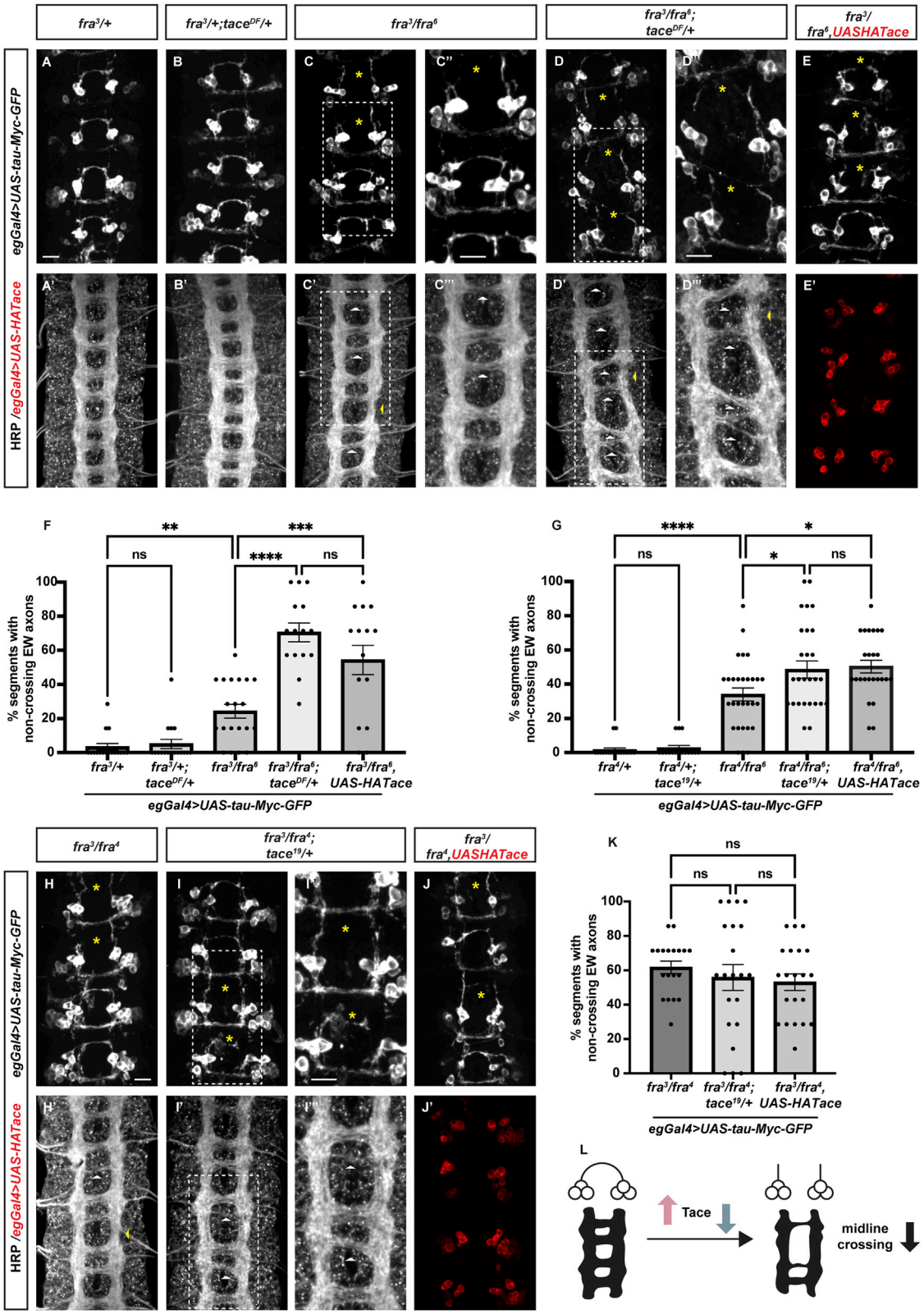

(legend on next page)

alleles, $tace^{CRISPR19}$ ($tace^{19}$) and $tace^{CRISPR17}$ ($tace^{17}$) (Figure S2A). Both alleles appear to be lethal, as adult escapers are rarely observed. In addition, in a combined population of 133 *tace* mutant embryos, 15 embryos (11.28%) exhibit defects in the midline guidance of eagle commissural axons (Figures 1J–1M). There are two clusters of eagle neurons, 3 EW neurons and 10–12 EG neurons, that project axons through the posterior and anterior commissure, respectively (Figure 1J).[34] Because the guidance of EW axons but not EG axons is dependent on the function of the Fra receptor,[35] we focused our analysis on the EWs. In these 15 *tace* mutant embryos, a significantly higher percentage of segments display EW projection defects compared with sibling controls, with many axons either stalling before reaching the contralateral side or ectopically extending ipsilateral projections (Figures 1K, 1L, and S2C). Abnormal midline crossing in these embryos is also readily observed in the axon scaffold, which was stained with the horseradish peroxidase (HRP) antibody (Figures 1K′ and 1L′). Phenotypes include thinning and breaks in commissures and longitudinal tracks, both of which are reminiscent of phenotypes observed in *fra* mutant embryos.[15] Together, these results suggest that *tace* is required for normal growth and midline crossing of commissural axons. Of note, we observe abnormal segmentation in some of the 15 *tace* mutant embryos, where the nerve cords either lack one or multiple segments or have displaced segment boundaries. At very low frequency, we also observe thickening of commissures that are indicative of ectopic crossings (Figure 1K′).

Due to the maternal deposition of *tace*, the low penetrance of the mutant phenotype is not unexpected (Figures S1A–S1E′). Indeed, a similar maternal effect is observed for other genes that control midline guidance, such as *son of sevenless* (*sos*), *kuzbanian* (*kuz*), and members of the Wave regulatory complex.[36–38] Our efforts to generate maternal zygotic *tace* mutants were unsuccessful, likely due to developmental arrest. To further investigate whether *tace* functions to promote midline crossing, we tested whether removing one copy of *tace* results in enhancement of midline crossing defects using the *fraΔC* sensitized genetic background. In this background, we express a dominant-negative form of the Fra receptor lacking its entire cytoplasmic domain (FraΔC) in eagle neurons.[35] This manipulation results in a failure of EW axons to cross the midline in approximately 30%–50% of segments (Figures 1N and 1R). Reducing the levels of *tace* in this background, either with a chromosomal deletion of *tace* ($tace^{DF}$) or in embryos that are heterozygous for $tace^{17}$ or $tace^{19}$, significantly increases EW axon non-crossing defects (Figures 1O–1R). As a control for specificity, we show that removing one copy of *kuz* (*kuzbanian*, *Drosophila* ADAM10, a highly related ADAM family member) does not alter the FraΔC-dependent EW non-crossing phenotype (Figures S2D–S2F). We also tested the effect of *tace* mutations in embryos heterozygous for both the repulsive receptor *robo1* and its ligand *slit*.[37,39] In these embryos, a decrease in Robo-mediated repulsion results in ectopic crossing of ipsilaterally projecting Fasciclin II (FasII)-positive axon fascicles (Figure S2H). Removing one copy of *tace* in this background suppresses the ectopic crossing defects (Figures S2I and S2J), further implicating *tace* as a positive regulator of midline guidance.

Unexpectedly, in embryos that strongly overexpress Tace, we also detected guidance defects in FraΔC and *slit*, *robo* backgrounds that are similar to those in *tace* heterozygous embryos (Figures 1S–1T and S2K–S2M). Because either reducing or increasing Tace levels negatively affects midline crossing (Figure 1U), this result suggests that, instead of functioning solely as a positive regulator, Tace has additional roles in midline guidance. We propose that stringent regulation of the abundance or activity of Tace is required for its optimal function and investigate this model further with the following experiments.

tace and *fra* function in the same pathway to promote midline crossing

Since Tace promotes midline crossing, we examined genetic interactions between *tace* and *fra* using different *fra* hypomorphic backgrounds to determine if they act in the same pathway. We used three *fra* alleles, the null fra^3 and fra^4 alleles and the hypomorphic fra^6 allele.[15,21] In stage 15–16 *fra*/+ heterozygous embryos or *fra*/+; *tace*/+ transheterozygotes, almost all EW axons cross the midline (Figures 2A, 2B, 2F, 2G, S3A, S3B, and S3F). Concordantly, the HRP-positive axon scaffold appears normal (Figures 2A′, 2B′, S3A′, and S3B′). In fra^3/fra^6 and fra^4/fra^6 hypomorphs, however, a significant population of EW axons fail to cross the midline (Figures 2C, 2F, 2G, and S3C), and some segments also show thinning or breaks in commissures or longitudinal axons (Figures 2C′ and S3C′). Removal of one copy of *tace* in *fra* hypomorphs with either the $tace^{DF}$ or the $tace^{19}$ allele significantly enhances EW axon crossing defects (Figures 2D, 2F, 2G,

Figure 2. *tace* genetically interacts with *fra*

(A–E′ and H–J′) Confocal micrographs show stage 15–16 *Drosophila* embryos of the indicated genotypes, with GFP labeling eagle neurons and HRP labeling all CNS axons.

(C–C‴) Mild midline crossing defects in EW axons (C, non-crossing axons indicated by asterisks) and HRP-labeled axon scaffolds (C′, thinned commissures indicated by triangles) are observed in fra^3/fra^6 hypomorphic mutants.

(D–D‴) Removing *tace* significantly enhances these phenotypes.

(H–I‴) Severe midline crossing defects in both EW axons and the HRP axon scaffold are observed in the fra^3/fra^4 amorphic mutants, which are not enhanced by the $tace^{19}$ allele.

(E–E′ and J–J′) Overexpression of Tace (red) in *fra* hypomorphic mutants (E, E′) but not in amorphic mutants (J, J′) enhances the EW axon non-crossing phenotype.

Regions outlined in dashed lines are magnified in (C″), (C‴), (D″), (D‴), (I″), and (I‴). Scale bars represent 10 μm. Anterior is up.

(F, G, and K) Quantification of the percentage of segments that have non-crossing EW axons in embryos of each indicated genotype. Number of embryos, n = 17, 17, 20, 15, 15 for (F), n = 18, 16, 29, 28, 25 for (G), n = 19, 21, 21 for (K). Statistical analysis was conducted with one-way ANOVA. Error bars indicate SEM; *p < 0.0332, **p < 0.0021, ***p < 0.0002, ****p < 0.0001.

(L) Schematic describing the phenotypes observed in the *fra* hypomorphic background.

and S3D). The increased severity of the phenotype is also evident in the axon scaffold (Figures 2D′ and S3D′), together supporting a role for *tace* in the *fra* pathway. Importantly, removing one copy of *tace* in fra^3/fra^4 null mutants results in no change in *fra*-dependent crossing phenotypes (Figures 2H–2I‴ and 2K), which is consistent with Tace and Fra functioning in the same pathway. In addition, decreasing the levels of *fra* in *tace* mutants also exacerbates the guidance defects (Figures S3H–S3K). Taken together, these results demonstrate that *tace* and *fra* function in the same genetic pathway.

Interestingly, similar to *tace* heterozygous embryos, overexpressing Tace in eagle neurons in *fra* hypomorphic backgrounds also results in significant enhancement of EW axon crossing defects (Figures 2E, 2E′, 2F, 2G, 2L, S3E, and S3E′). This gain-of-function phenotype precludes us from rescuing the EW non-crossing phenotype (Figure S3G), yet this result provides additional support for our model that Tace levels or activity must be tightly controlled. In contrast, overexpressing Tace in the fra^3/fra^4 null mutants does not enhance EW axon non-crossing defects (Figures 2J and 2K). As ADAMs have many substrates, manipulating Tace levels could have an impact on Fra-independent pathways that are also required for midline crossing; however, the fact that neither overexpressing nor removing *tace* enhances non-crossing phenotypes in *fra* null mutants strongly suggests that Tace acts specifically in the Fra pathway.

Tace binds to Fra and cleaves Fra

To determine whether Fra is a Tace substrate, we tested if Tace could cleave Fra in *Drosophila* S2R+ cells, which express minimal levels of endogenous Tace.[40] In S2R+ cells transfected with N-terminal hemagglutinin (HA)-tagged Fra, we observe low baseline release of Fra ECDs into the medium supernatant (Figure 3A). However, cotransfection of Tace induces significant increases in the release of cleaved Fra ECDs and a marked reduction in full-length Fra in the cell lysate (Figure 3A). In contrast, cotransfection of an enzymatically dead variant of Tace that lacks the autoinhibitory prodomain and the catalytically active metalloprotease domain (TaceΔMP) does not induce Fra ECD cleavage (Figure 3A). TaceΔMP acts as a dominant negative, since it retains its ability to bind to its substrate (Figure 3D) but is enzymatically inactive.[41] Accordingly, cotransfection of TaceΔMP with full-length Tace completely blocks Tace-dependent Fra ECD cleavage (Figure 3A). Notably, Tace induces the formation of two Fra ECD fragments: a larger fragment that is approximately 110 kDa in molecular weight and a smaller fragment of approximately 50 kDa (Figures 3A and 3C). Taken together, these observations demonstrate that Tace induces the cleavage of Fra ECDs.

In the non-canonical pathway, Fra is processed by γ-secretase to release a transcriptionally active ICD that promotes midline crossing by inducing *comm* expression.[1] Structural and functional evidence indicates that γ-secretase cleavage occurs constitutively once the ECD of the substrate is released.[42] In addition, all four members of the γ-secretase complex (*psn*, *pen-2*, *nct*, *aph-1*) are expressed at high levels in S2R+ cells.[40] Therefore, we predicted that Tace expression should induce Fra ICD cleavage. Indeed, we observe significant increases in the levels of Fra ICDs in cells cotransfected with full-length Tace but not in cells that express TaceΔMP (Figure 3B). In addition to the 50 kDa Fra ICD fragment, we observe two additional Myc-labeled fragments in the cell lysate. One fragment is approximately 115 kDa (Fra stub B), and the second fragment is slightly larger than the Fra ICD (Fra stub A). Since the levels of both Fra stub A and Fra stub B are visibly elevated only when Tace is present (Figure 3B), it is reasonable to assume that these fragments correspond to the remaining portion of Fra after the release of Fra ECD A and Fra ECD B, respectively (Figure 3C). Expression of increasing levels of Tace leads to a dose-dependent increase in Fra cleavage (Figures S4A and S4B). Moreover, Kuz cannot induce the formation of the Fra ECD B and Fra ICD (Figures S4C and S4D). Together, these results support the specificity of Fra cleavage by Tace.

To determine if Tace physically interacts with Fra, we performed coimmunoprecipitation assays using lysates from both S2R+ cells (Figure 3D) and *Drosophila* embryos that pan-neurally express tagged Fra and Tace (Figure 3E) and found that Tace binds to Fra. Overexpression of Tace in these embryos also increases the levels of the Fra ICD compared with overexpression of a membrane-targeted GFP control (Figure 3E). While this increase is detectable in embryonic lysates collected from a mixed population of both early- and late-stage embryos (collected 24 h post-egg laying), we detect more abundant levels of the Fra ICD in stage 13–14 embryos (collected 9–12 h post-egg laying). This suggests that Tace-dependent Fra cleavage likely occurs primarily at the developmental stage when commissural neurons are sending their axons across the midline, which is consistent with a role for Tace in the non-canonical Fra pathway that is activated specifically during this narrow developmental window.[1]

tace acts in the non-canonical Fra pathway and is required for *comm* expression

In the non-canonical Fra pathway, Fra is cleaved by γ-secretase to form the transcriptionally active Fra ICD, which translocates to the nucleus to induce *comm* expression.[1,21] To assess whether Tace acts specifically in this pathway, we tested whether *tace* genetically interacts with *psn* and *comm.* In stage 16 embryos that are heterozygous or mutant for *tace*, EW axons occasionally extend aberrant projections that protrude from the side of the main EW commissural axon bundles (Figures 4A, 4B, 4F, and S3L). These projections deviate from the trajectory of the main axon bundles and often project ipsilaterally or away from the midline (Figures 4A′ and 4B′). Because six EW neurons from both hemisegments are labeled, it is unclear whether these aberrant projections defasciculate before or after crossing the midline. In either case, defasciculation reflects defects in commissural axon guidance. To determine if this phenotype is dependent on the function of Fra, we tested if reducing the level of *fra* in *tace* heterozygotes or mutants would increase the occurrence of such defasciculation events. Indeed, both *fra*/+; *tace*/+ transheterozygotes and *fra*/+; *tace* embryos show more severe phenotypes (Figures 4C, 4F, and S3L), again demonstrating that *fra* and *tace* function in the same pathway to regulate commissural axon guidance. Removing one copy of either *psn*

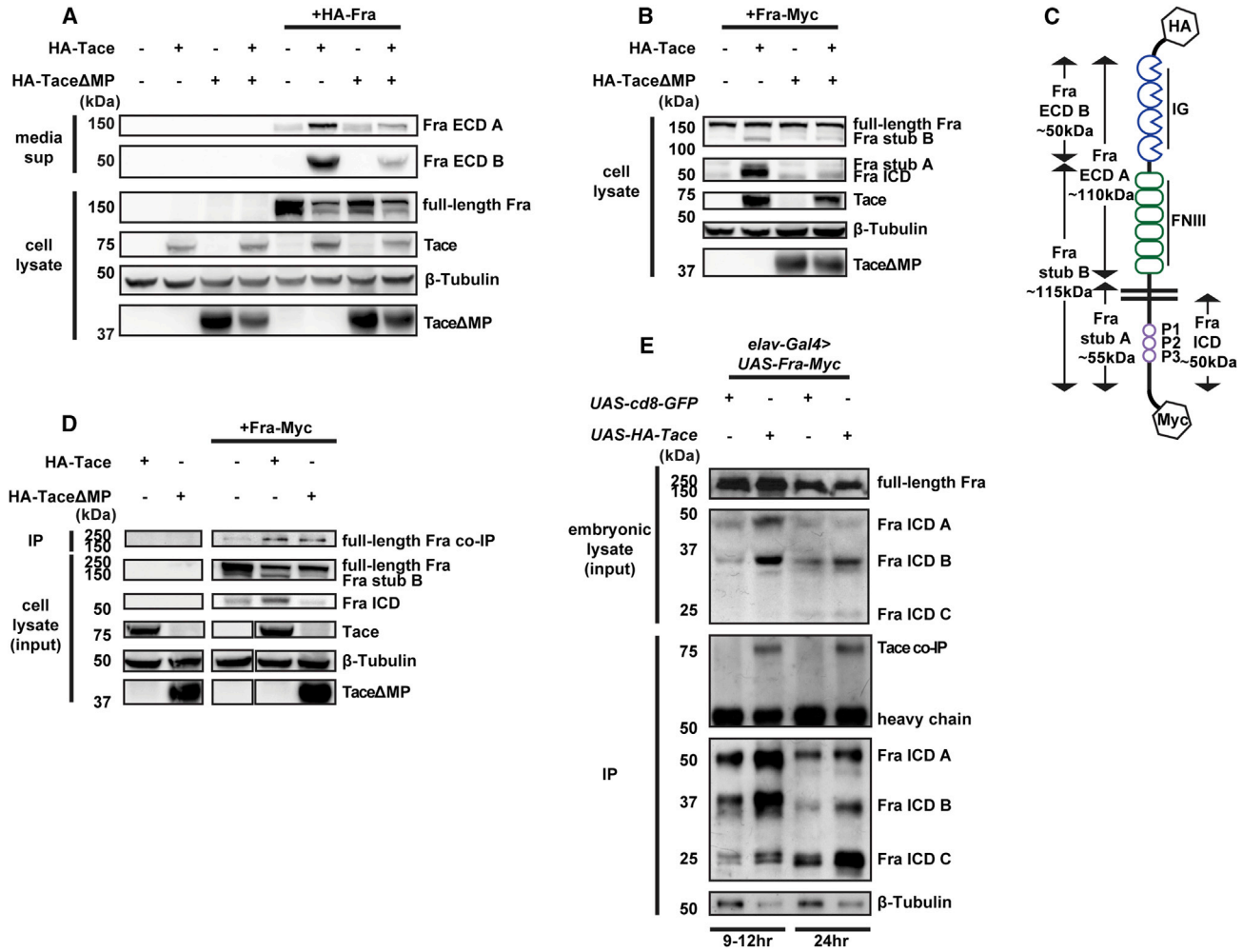

Figure 3. Tace physically interacts with Fra and induces cleavage

(A and B) Cell lysates and medium supernatants were prepared from *Drosophila* S2R+ cells transiently transfected with (A) an N-terminally HA-tagged Fra to monitor Fra ECD cleavage products or (B) a C-terminally Myc-tagged Fra to monitor cleaved Fra ICD fragments.

(C) Schematic representing Fra cleavage fragments observed in the S2R+ cell line.

(D) Immunoprecipitation was performed with an anti-HA antibody in cell lysates obtained from *Drosophila* S2R+ cells transiently transfected with the indicated constructs.

(E) Protein extracts were prepared from *Drosophila* embryos pan-neurally co-overexpressing C-terminally Myc-tagged Fra, with either a membrane-tethered GFP (cd8-GFP) or an HA-tagged Tace, using the *elav-Gal4* driver. Embryos were collected either 9–12 or 24 h post-egg laying. Immunoprecipitation was performed in embryonic lysates with an anti-Myc antibody.

or *comm* in *tace* mutants results in a phenotype that bears strong resemblance to removing one copy of *fra* (Figures 4D–4F). This result demonstrates that *tace* genetically interacts with known components of the non-canonical Fra pathway, which strongly supports a role for Tace in this pathway (Figure 4G).

Our biochemical data have established that Tace can induce the formation of the Fra ICD (Figures 3B and 3E). Thus, we expect decreased levels of Fra ICD in *tace* mutant embryos and a corresponding decrease in *comm* expression. To test this idea, we selected embryos at stage 14 for analysis, which is when most commissural axons are crossing the midline and when *comm* expression is highest.[1,21,22] Compared with *tace* heterozygous sibling controls, *tace* mutant embryos show significantly fewer EW neurons expressing *comm* (Figures 4H–4J). The decrease in *comm* expression seen in *tace* mutants (Figure 4J) closely mirrors what has been reported for *fra* mutants[1] and further supports our argument that Tace is an upstream regulator of Fra. In addition to the EW neurons, *comm* is also expressed in other populations of commissural neurons.[22] Thus, we quantified the overall *comm* expression level in the abdominal segments of the nerve cord and observed a significant decrease when *tace* is removed (Figure 4K), further supporting the conclusion that *tace* is required to regulate *comm* expression (Figure 4L). Taken together, these results strongly support a role for Tace in the non-canonical Fra pathway to induce *comm* expression (Figure 4L) and promote midline crossing (Figure 4G).

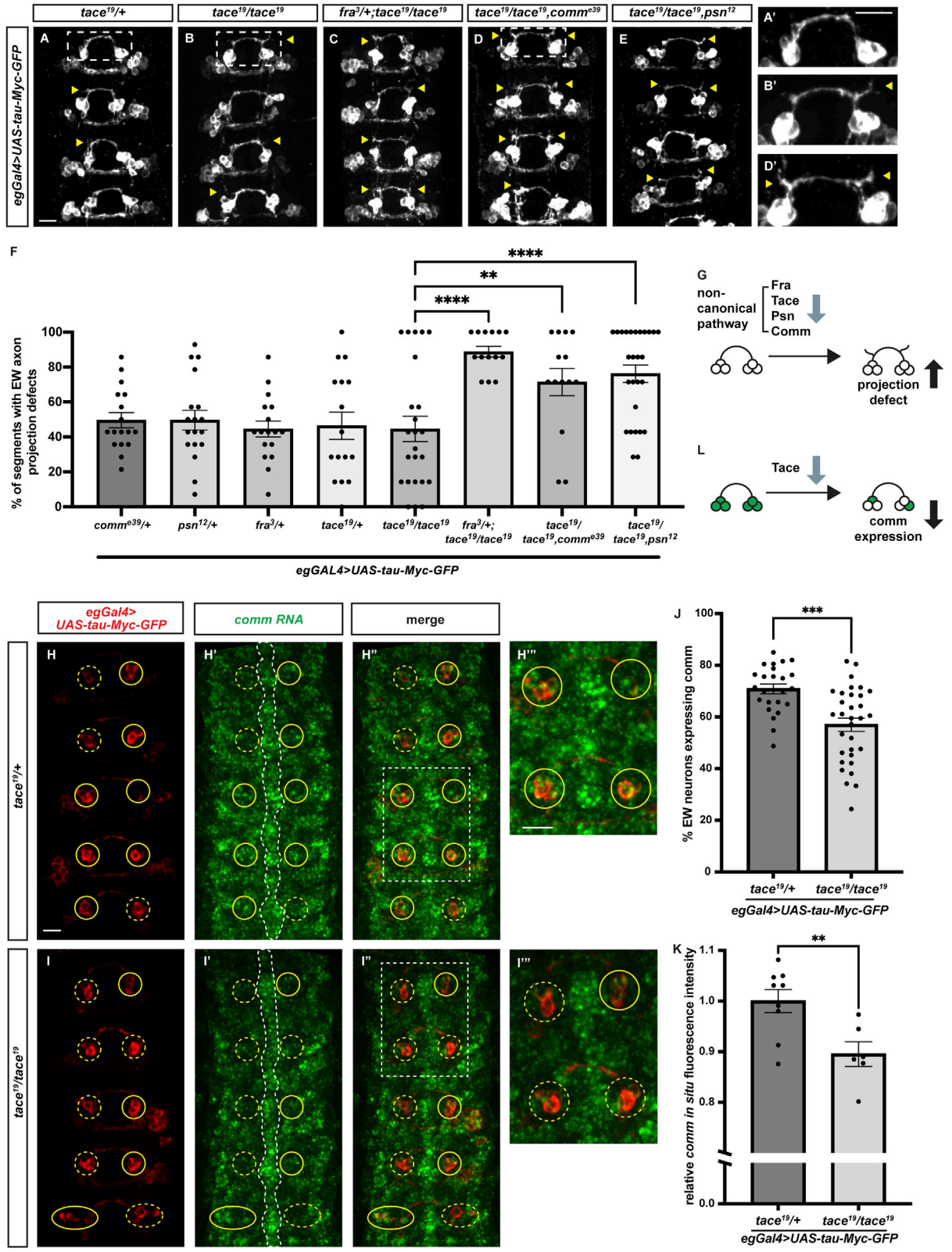

(legend on next page)

Overexpression of Tace inhibits netrin responses

Our results in the FraΔC and *fra* hypomorphic backgrounds unexpectedly revealed that both reducing and increasing *tace* levels negatively affect midline crossing of commissural axons (Figures 1U and 2L). How could increasing Tace levels result in commissural guidance defects? We speculated that overexpressed Tace could function in either a netrin-dependent or a netrin-independent manner. To distinguish between these possibilities, we overexpressed Tace in *netrinAB* (*netAB*) double mutants and observe that, while Tace overexpression enhances midline crossing defects in EW axons in *fra* hypomorphs (Figures 2F and 2G), it has no effect in *netAB* mutants (Figures S5A–S5D). This result suggests that overexpressed Tace acts by inhibiting netrin function. We further hypothesized that overexpressed Tace results in excessive cleavage of the Fra ECD, which would render neurons unable to respond to netrin correctly. To test this idea *in vivo*, we first determined whether Tace overexpression leads to a reduction in the amount of full-length Fra receptor. To measure this, we used an endogenously tagged Fra that has a GFP tag in the ECD and compared the normalized abundance of Fra on CNS axons in the presence and absence of Tace overexpression (Figures S5E and S5F).[43] Indeed, when we pan-neurally overexpress Tace, we observe a significant reduction in endogenous Fra levels (Figure S5G).

Next, we tested whether Tace overexpression can suppress netrin responses *in vivo*. *apterous-Gal4* labels a restricted population of ipsilaterally projecting interneurons (ap neurons) that express low levels of Fra.[44] In wild-type embryos, ap axons do not cross the midline (Figures 5A and 5A′). Tace overexpression alone in ap neurons does not induce ectopic crossing (Figures 5B and 5B′). In contrast, overexpressing Fra causes a significant increase in the number of segments with ectopic crossing of these axons (Figures 5C, 5E, 5G, and 5H). This phenotype depends primarily on the interaction between Fra and netrin, as the ectopic crossing phenotype is almost completely suppressed in *netAB* mutants (Figures 5F and 5H). Thus, we can use this Fra gain-of-function assay to quantitively measure netrin-mediated Fra responses. We find that when both Tace and Fra are overexpressed in ap neurons, Tace significantly suppresses the Fra gain-of-function phenotype (Figures 5D, 5D′, and 5G). This observation supports the idea that Tace overexpression suppresses midline crossing by inhibiting Fra's response to netrin (Figure 5I).

Together, our data support a model in which Tace cleavage of Fra activates the netrin-independent non-canonical pathway, while inhibiting the netrin-dependent canonical pathway. Because both pathways are required in commissural neurons at the time of crossing, inhibition of either pathway is detrimental to appropriate midline guidance, and activation of any one pathway is not sufficient to drive midline crossing. As such, Tace may act at this important developmental time point to instruct the neuron to switch and balance the two pathways.

ADAM17 plays a conserved role in binding and cleaving Dcc

To test whether ADAM17 has a conserved role in processing the Fra vertebrate homolog Dcc, we first performed cleavage assays in S2R+ cells with rat Dcc and *Drosophila* Tace. Cotransfection of Tace induces both Dcc ECD and ICD cleavage and results in significantly decreased levels of full-length Dcc (Figure 6A). These effects were not observed in cells cotransfected with TaceΔMP (Figure 6A). To investigate the role of ADAM17 in a mammalian cell context, we used the HEK293T cell line, which expresses ADAM17 endogenously.[45] In 293T cells, Dcc ECD is constitutively cleaved and released in the medium supernatant. This cleavage is significantly enhanced when the cells are stimulated by the phorbol ester phorbol 12-myristate 13-acetate (PMA), a specific and potent activator of ADAM17 (Figures 6B and 6C).[46] We then used a series of metalloprotease inhibitors, including (1) GM6001, which inhibits matrix metalloproteases (MMPs) and several ADAMs; (2) TAPI-1, which inhibits ADAM17 with high specificity, along with MMPs; (3) the ADAM10-specific inhibitor GI254023X; and (4) GM1489, a broad-spectrum MMP inhibitor.[29,47] Importantly, we observe that the PMA-induced Dcc cleavage is completely abolished by GM6001 and TAPI-1, while GM1489 and GI254023X show no effect, demonstrating that ADAM17 specifically cleaves Dcc (Figures 6B and 6C). In addition to promoting Dcc cleavage, both full-length Tace and TaceΔMP physically interact with

Figure 4. *tace* genetically interacts with components of the non-canonical Fra pathway and is required for *comm* expression

(A–G) Stage 16 *Drosophila* embryos, with GFP labeling eagle commissural neurons.

(A and B) EW axons that defasciculate and project either ipsilaterally or away from the main EW axon bundles are observed in heterozygous or homozygous *tace* mutants (indicated by yellow triangles).

(C–E) fra^{3}, $comm^{\Delta e39}$, and psn^{12} alleles significantly enhance these phenotypes. Regions outlined by dashed lines are magnified in (A′), (B′), and (D′).

(F) Quantification of the percentage of segments that have EW axon projection defects. Number of embryos, n = 17, 18, 17, 16, 24, 14, 14, 27. Statistical analysis was conducted with one-way ANOVA.

(G) Schematic describing the phenotypes observed.

(H–L) Stage 14 *Drosophila* embryos, with RNA FISH for *comm* shown in green and eagle neurons labeled in red. *comm* transcripts are detected at the midline (H′ and I′, white dotted lines) and in the cell bodies of eagle neurons (H–I‴, eagle neurons are outlined in solid yellow circles if expressing *comm* and in dotted yellow circles if not expressing *comm*).

(H″ and I″) Regions outlined in dashed lines are magnified in (H‴) and (I‴).

(J) Quantification of the percentage of eagle neurons that express *comm*. Number of embryos, n = 24, 32. Statistical analysis was conducted with Student's t test.

(K) Quantification of the relative fluorescence intensity of *comm* RNA FISH signal normalized to the average fluorescence intensity of *comm* RNA FISH signal at the midline. Number of embryos, n = 9, 6. Statistical analysis was conducted with Student's t test.

(L) Schematic describing the phenotypes observed. In all micrographs, anterior is up and scale bars represent 10 μm. Error bars indicate SEM; $^{**}p < 0.0021$, $^{***}p < 0.0002$, $^{****}p < 0.0001$.

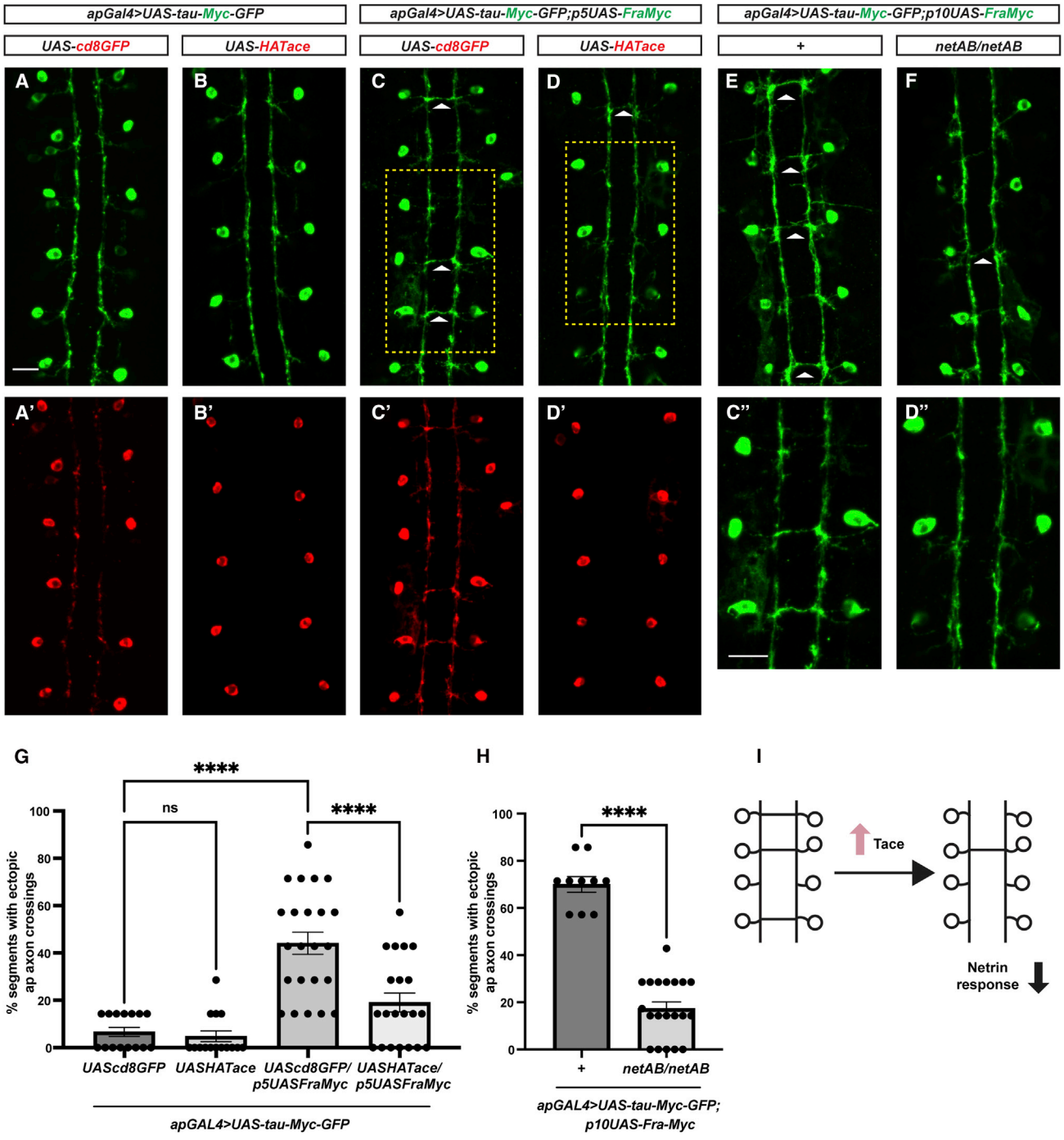

Figure 5. Overexpression of Tace inhibits netrin response in *Drosophila* embryos

(A–F) Stage 17 *Drosophila* embryos that carry *apGal4* to label ipsilaterally projecting ap neurons and their axons with a Myc tag (A–F, green), a GFP tag (A′ and C′, red), and an HA-tagged Tace (B′ and D′, red).

(A and B) Expressing the GFP tag or Tace does not cause ectopic crossing.

(C and D) Expressing *p5UAS-Fra-Myc* induces a significant increase in ectopic crossing (C), which is significantly suppressed by overexpression of Tace (D). Regions in dashed lines are magnified in (C″) and (D″).

(E and F) Expressing *p10UAS-Fra-Myc* induces a significant increase in the percentage of ectopic crossing (E), which is significantly suppressed in the absence of *netrin* (F). White triangles indicate ectopic crossing. Scale bars represent 10 μm. Anterior is up.

(G and H) Quantification of the percentage of segments with ectopic crossing. Number of embryos, n = 15, 15, 23, 21 for (G), n = 10, 20 for (H). Statistical analysis was conducted with one-way ANOVA in (G) and Student's t test in (H). Error bars indicate SEM; ****$p < 0.0001$.

(I) Schematic describing the phenotypes observed in ap axons.

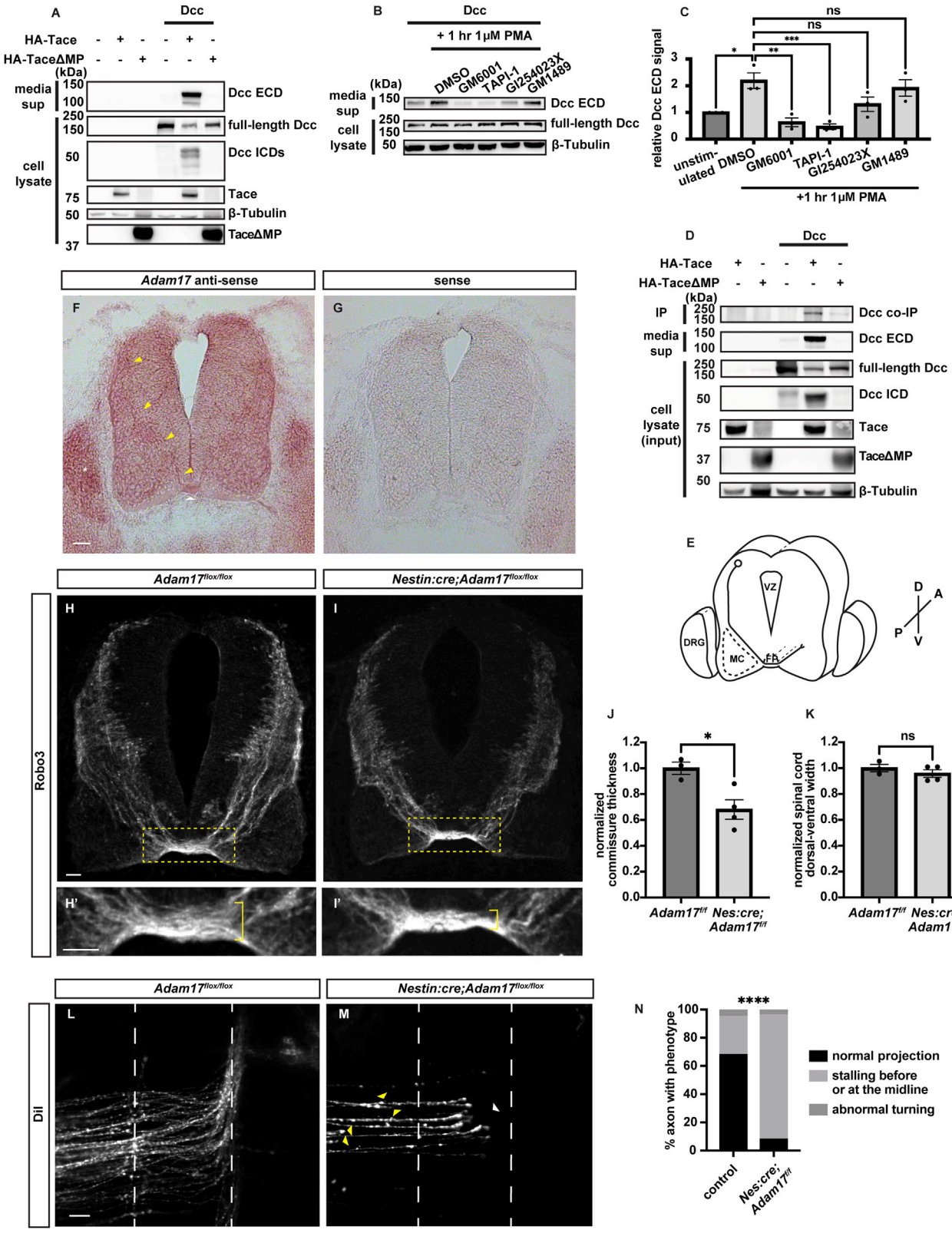

(legend on next page)

Dcc in S2R+ cells (Figure 6D). Taken together, our biochemical results strongly suggest that Tace and ADAM17 play a conserved role in the proteolytic release of the Fra and Dcc ECDs and that this initial cleavage is sufficient to induce subsequent γ-secretase-mediated ICD cleavage.

Conditional removal of *Adam17* disrupts commissural axon guidance in the spinal cord

To evaluate the function of ADAM17 in regulating midline crossing, we first examined its expression pattern in the developing mouse spinal cord by performing RNA *in situ* hybridization using an antisense probe against *Adam17* (Figure 6F) and a sense probe against *Ndfip1* previously characterized to have no background staining as a negative control (Figure 6G).[48] *Adam17* transcripts are broadly expressed in E11.5 spinal cord and the dorsal root ganglion (DRG), in regions including the motor column (MC), the floor plate (FP), and along the commissural axon tracks (Figures 6E and 6F).

Since *Adam17* is expressed in the spinal cord at E11.5, which is when commissural axons are crossing the floor plate, we investigated the role of ADAM17 in commissural axon guidance by generating *Adam17* conditional knockout (cKO) embryos, using an *Adam17* floxed line.[49] Since Tace is broadly expressed in the spinal cord, we chose the *Nestin1:cre* (*Nes:cre*) line,[49] which expresses the Cre recombinase in both neuronal and glial precursors starting sparsely at E9 and covering the entire spinal cord at E11.[50] We validated the conditional removal of Tace by PCR and qRT-PCR (see STAR Methods and Figures S6A–S6D). Next, we analyzed commissural axon guidance defects in *Adam17* cKO embryos by performing Robo3 (a specific commissural axon marker) immunostaining in transverse sections of E11.5 spinal cords (Figures 6H–6I′). Compared with control embryos, the thickness of Robo3-positive commissures at the ventral midline is significantly reduced in *Adam17* cKO embryos, demonstrating that ADAM17 is required *in vivo* for the midline crossing of commissural axons (Figure 6J). In contrast, the dorsal-ventral width of spinal cords remains unchanged, indicating that the cKOs do not exhibit gross developmental delay (Figure 6K).

To determine whether neuronal differentiation, patterning, and cell death are affected in *Adam17* cKO spinal cords, we used Brn3a (which labels the dI1, dI2, dI3, and dI5 neuronal populations), Lhx1/5 (which labels the dI2, dI4, and dI6 and V0 and V1 neuronal populations), and cleaved caspase-3 (apoptosis marker) as markers (Figure S6E). Robo3-positive commissural neurons compose substantial fractions of the dI1, dI2, dI4, dI5, dI6, and V0 populations.[51] Importantly, we observe no difference in Brn3a and Lhx1/5 expression in *Adam17* cKO spinal cords compared with controls (Figures S6F–S6I, S6L, and S6M), suggesting that the thinning of the Robo3-positive commissure that we observe in *Adam17* cKO embryos (Figures 6H–6J) is unlikely to be a result of abnormal neuronal differentiation. Further, we observe few cells positive for cleaved caspase-3 in *Adam17* cKO spinal cords, suggesting that abnormal cell death is unlikely to contribute to the reduction in commissure thickness (Figures S6J and S6K).

To characterize the axon projection defects in *Adam17* cKO embryos in more detail, we performed a series of unilateral 1,1′-dioctadecyl-3,3,3′3′-tetramethylindocarbocyanine perchlorate (DiI) dye injections to analyze the behavior of individual and small subsets of commissural axons (Figure S6N). In control embryos, most labeled axons extend to the floor plate, cross the midline, and then project anteriorly (Figure 6L). In *Adam17* cKO embryos, however, we observe a significant increase in the percentage of labeled axons that stall either before reaching the floor plate or at the midline (Figures 6M and 6N). This assay thus allowed us to show on a single-axon level that commissural axons in *Adam17* cKO embryos frequently fail to project to the contralateral side, which is consistent with the observed reduction in commissure thickness (Figure 6I′ and 6J). Together, these results demonstrate that ADAM17 is required for midline crossing in the embryonic mouse spinal cord, which is highly reminiscent of the phenotypes observed in *tace* mutants in *Drosophila.*

ADAM17 regulates netrin responses in commissural neurons

In *Drosophila*, we have shown that overexpressing Tace inhibits Fra gain of function by suppressing the receptor's ability to respond to netrin (Figure 5). Does elevated ADAM17 expression

Figure 6. ADAM17 binds to and cleaves Dcc and is required for commissural axon midline crossing in the developing mouse spinal cord

(A) Cell lysates and medium supernatants prepared from *Drosophila* S2R+ cells transfected with the indicated constructs.

(B) Cell lysates and medium supernatants prepared from HEK293T cells transiently transfected with Dcc. When indicated, HEK293T cells were stimulated for 1 h with 1 μM PMA. At the same time, different metalloprotease inhibitors, or DMSO as vehicle control, were applied to the cells.

(C) Quantification of band intensities of Dcc ECD in the medium supernatant under the indicated conditions, normalized to Dcc ECD in the unstimulated condition. Band intensities of Dcc ECD were further normalized to band intensities of β-tubulin. Number of independent assays, n = 3. Statistical analysis was conducted with one-way ANOVA.

(D) Immunoprecipitation was performed with an anti-HA antibody in cell lysates obtained from S2R+ cells transiently transfected with the indicated constructs.

(E) Schematic depicting the structure of the embryonic mouse spinal cord, the DRG, and the trajectory of a commissural axon.

(F and G) The expression of *Adam17* transcript shown by *in situ* hybridization on E11.5 mouse spinal cord, with an antisense probe against *Adam17* (F) and a sense probe against *Ndfip1* (G) as a control. Asterisk marks the DRG, white arrow marks the FP, and yellow arrows mark the trajectory of commissural axons. DRG, dorsal root ganglion; MC, motor column; FP, floor plate; VZ, ventricular zone.

(H–I′) Immunostaining of Robo3 in transverse sections of E11.5 mouse spinal cords. The regions outlined in yellow dashed lines are shown at higher magnification in (H′) and (I′). Scale bars represent 40 μm. Dorsal is up.

(J and K) Quantification of normalized commissure thickness (J) and spinal cord dorsal-ventral width (K) in E11.5 mouse embryos. Number of embryos, n = 3, 4 for (J), n = 3, 4 for (K). Statistical analysis was conducted with Student's t test.

(L–N) 1,1′-dioctadecyl-3,3,3′3′-tetramethylindocarbocyanine perchlorate (DiI)-filled commissural axons cross the midline and project anteriorly in control embryos (L), but frequently stall before reaching the floor plate (indicated by yellow triangles) or at the midline (indicated by the white triangle) in *Adam17* cKO embryos (M). Scale bar represents 40 μm. Anterior is up. The percentage of axons with the indicated phenotype is quantified in (N). Number of injection sites, n = 72, 33. Statistical analysis was conducted with chi-square analysis. Error bars indicate SEM; *p < 0.0332, **p < 0.0021, ***p < 0.0002, ****p < 0.0001.

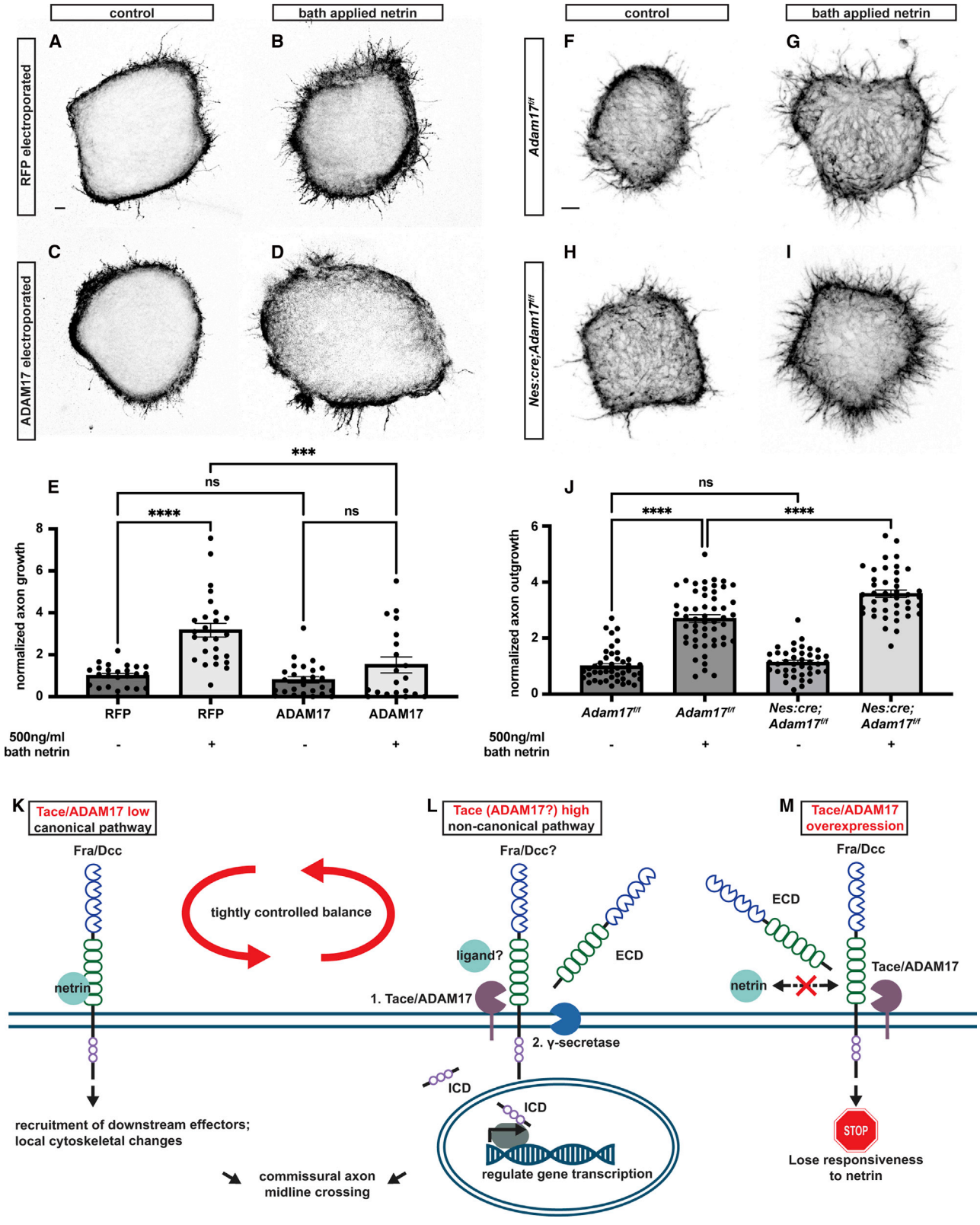

(legend on next page)

result in a similar disruption in netrin responses in vertebrates? To address this question, we electroporated E12.5 mouse spinal cords with HA-tagged ADAM17 or an empty vector, along with cytosolic RFP to monitor electroporation efficiency (Figures S7A–S7B″). The spinal cords were then cut into explants, embedded in collagen gel, and cultured next to mock 293T cell aggregates or 293T cell aggregates expressing netrin (Figures S7C–S7E). To verify the commissural identity of these explants, we dissociated them into primary neuronal cultures and observe that most dissociated neurons are positive for the commissural marker Robo3. Further, HA-positive electroporated neurons almost always colocalize with Robo3 (Figures S7F–S7I″). Our ADAM17-electroporated explants and control explants show comparable numbers of RFP-positive cells, demonstrating equivalent electroporation efficiency (Figures S7A–S7B″). Control explants, when cultured next to mock cell aggregates, show minimal axonal outgrowth on all sides of the explants (Figure S7J). However, when cultured next to netrin-expressing cell aggregates, control explants show increased axonal outgrowth on the side that is facing netrin (Figure S7K). This difference is reflected in the increased proximal-to-distal ratio of axonal outgrowth (Figure S7N), which is consistent with previous reports demonstrating that netrin promotes axonal outgrowth.[52] When cultured next to mock cell aggregates, ADAM17-electroporated explants show a similar proximal-to-distal ratio of axon outgrowth compared with control explants (Figures S7L and S7N), indicating that ADAM17 alone does not induce changes in axonal outgrowth. Importantly, the netrin-dependent increase in axon outgrowth is abolished in ADAM17-electroporated explants, suggesting that ADAM17 overexpression inhibits netrin responses (Figures S7M and S7N).

To corroborate this result, we also tested whether ADAM17 electroporation would show a similar inhibitory effect in response to bath application of recombinant netrin. Without netrin stimulation, control explants and ADAM17-electroporated explants both show very little axonal outgrowth (Figures 7A, 7C, and 7E). In contrast, bath application of recombinant netrin induces a significant increase in axonal outgrowth in control explants (Figures 7B and 7E). However, ADAM17 electroporation significantly suppresses the netrin-induced increase in outgrowth (Figures 7D and 7E). Together, our data from both Tace overexpression in *Drosophila* ap neurons (Figure 5) and ADAM17 overexpression in mouse spinal cord explants (Figures 7A–7E and S7J–S7N) demonstrate that Tace/ADAM17 overexpression inhibits axonal responses to netrin.

We next asked whether ADAM17 also regulates netrin responses in commissural axons at its physiological expression level. In *Adam17* cKO explants, we predicted that the absence of ADAM17-dependent cleavage should lead to increased levels of Dcc, which would result in enhanced netrin-mediated axon outgrowth compared with control explants. Indeed, while we observe no difference in netrin response in the absence of bath-applied netrin (Figures 7F, 7H, and 7J), in the presence of netrin we observe a significant increase in axon outgrowth in *Adam17* cKO explants compared with control explants (Figures 7G, 7I, and 7J). Importantly, this result provides direct evidence for ADAM17's function in regulating the netrin-dependent canonical pathway.

Together, our results show striking functional conservation between Tace and ADAM17. Similar to the conflicting phenotypes we observed with loss and gain of Tace in *Drosophila* (Figures 1, 2, and S2), in the developing mouse spinal cord, genetic ablation of *Adam17* and overexpression of ADAM17 both result in disruptions in the growth and guidance of commissural axons (Figures 6 and 7). Furthermore, we also showed in mice that ADAM17 directly modulates netrin responses in commissural neurons. These observations strongly support a role for ADAM17 in both a netrin-dependent and a netrin-independent pathway. Because the non-canonical pathway has not been established for Dcc at the vertebrate midline, our results thus provide evidence that this signaling mechanism may be evolutionarily conserved.

DISCUSSION

Here we report a conserved role for Tace and ADAM17 in coordinating different receptor signaling outputs. In the context of commissural axon guidance, we provide strong biochemical and genetic evidence demonstrating that Tace functions in both the canonical netrin-dependent Fra pathway and the non-canonical netrin-independent Fra pathway. Specifically, we have shown that in the non-canonical pathway, Tace cleaves Fra to induce the formation of a transcriptionally active ICD fragment that regulates the expression of Fra's target gene *comm*

Figure 7. ADAM17 bi-directionally regulates netrin responses in commissural axons

(A–J) E12.5 mouse dorsal spinal explants labeled with β-tubulin antibody to visualize axon outgrowth. Normalized axon growth was measured as the total axon outgrowth that is present across the entire circumference of each explant. The measurements were normalized to the circumference of the explant and further normalized to the control condition. Scale bars represent 20 μm.

(A–D) Explants were electroporated with the indicated constructs and cultured with (B and D) or without (A and C) bath application of 500 ng/μL recombinant netrin.

(E) Quantification of axon growth in (A–D). Number of explants, n = 25, 26, 26, 20.

(F–I) Explants were harvested from control (F and G) or *Adam17* cKO (H and I) embryos and cultured with (G and I) or without (F and H) bath application of 500 ng/μL recombinant netrin.

(J) Quantification of axon growth in (F–I). Number of explants, n = 44, 53, 41, 42. All statistical analyses were conducted with one-way ANOVA. Error bars indicate SEM; ***$p < 0.0002$, ****$p < 0.0001$.

(K–M) A model for the function of Tace/ADAM17 in commissural axon guidance.

(K) When the levels or activities of Tace or ADAM17 are low, commissural neurons favor the canonical pathway to promote midline attraction.

(L) In *Drosophila*, when Tace is activated, commissural neurons switch to the non-canonical Fra pathway to facilitate midline crossing. It is unclear if Dcc has a similar non-canonical pathway that is regulated by ADAM17.

(M) When Tace or ADAM17 is overexpressed, the excessive proteolysis of the Fra or Dcc receptor may inhibit productive interaction with netrin.

(Figure 7L). In the canonical pathway, overexpression of Tace results in excessive cleavage of Fra that inhibits the receptor's ability to respond to netrin (Figures 7K and 7M). Because both Fra pathways are essential for proper midline attraction, such bidirectional regulation by Tace could assist the neurons in orchestrating appropriate signaling outputs. Thus, we propose a model in which the levels and/or activity of Tace must be correctly regulated to ensure that Fra signals effectively. When the levels or activities of Tace are low, the commissural neuron favors the netrin-dependent canonical pathway to promote midline crossing (Figure 7K). In contrast, when Tace is activated, the commissural neuron decreases its responsiveness to netrin and switches to the non-canonical Fra pathway to regulate gene transcription (Figure 7L). Together, these two pathways are maintained in a tightly controlled balance and cooperate to facilitate commissural axon midline crossing. Importantly, we also demonstrated a clear functional similarity between Tace and ADAM17, arguing that ADAM17-dependent cleavage of Dcc likely allows for a similar segregation of receptor signaling outputs in vertebrate systems.

Tace regulates the non-canonical Fra pathway

Previous studies have revealed that ADAM-dependent proteolysis can impinge on downstream signaling pathways of guidance receptors in many ways. First, ADAM cleavage can terminate receptor signaling by reducing receptor surface levels.[53] Second, ADAM cleavage can facilitate association between the receptor and its downstream effector proteins.[38] Third, ADAM cleavage can physically separate receptor-ligand complexes to switch adhesion to repulsion.[54] Previous studies have demonstrated that both of Fra's vertebrate homologs, Dcc and neogenin, are also ADAM substrates,[32,55–57] yet the physiological significance and the precise mechanisms of how proteolysis affects downstream signaling of these receptors remain unclear. In this study, we have shown that in *Drosophila*, Tace induces the formation of both Fra ECDs and ICDs and is required for the expression of Fra's transcriptional target gene *comm.* Unlike the mechanisms described above, our data establish a distinct pathway in which an ADAM can activate an axon guidance receptor by initiating subsequent γ-secretase cleavage to induce transcriptional activity of the receptor.

It remains to be seen whether the same non-canonical mechanism is conserved for ADAM17 and Fra's vertebrate homologs Dcc and neogenin. In *Drosophila* commissural neurons, γ-secretase cleaves Fra to generate an ICD fragment, allowing it to translocate to the nucleus to regulate the transcription of *comm*.[1] Previous studies have demonstrated that the neogenin ICD is present in the nucleus in both chick retinal ganglion cells and zebrafish embryos.[58,59] In addition, *in vitro* evidence from cell lines suggests that both neogenin and Dcc ICDs can localize to the nucleus to modulate gene transcription, suggesting that similar non-canonical pathways exist for Dcc and neogenin as well.[24,25] We have shown that conditional removal of *Adam17* disrupts midline crossing *in vivo.* If the only function of ADAM17 at the vertebrate midline is to downregulate netrin and Dcc signaling, we would expect to see increased crossing when ADAM17 levels are reduced. Thus, in vertebrates, ADAM17 behaves similarly to Tace in *Drosophila* to positively regulate midline crossing. This observation supports a potential role for ADAM17 in activating the transcriptional activities of Dcc at the vertebrate midline.

While Dcc is arguably the most likely substrate, it should be noted that our analysis in embryonic mouse spinal cords does not exclude the possibility that ADAM17 functions by regulating other substrates. One possibility is neogenin, which, in addition to netrin, also binds to its canonical ligand repulsive guidance molecule (RGM) with much higher affinity.[60] Cleavage of neogenin by ADAM17 desensitizes axons to RGM, which abolishes its repulsive effects on neurite outgrowth.[55,57] Importantly, neogenin contributes to commissure formation in the mouse spinal cord by binding and facilitating Dcc and netrin signaling through its ECDs.[61] Thus, we argue it is unlikely that neogenin is the primary ADAM17 substrate, as shedding of its ECDs should have deleterious effects on midline guidance, which is contrary to what we observed in *Adam17* cKO embryos (Figures 7E–7L). Another possible substrate is the repulsive receptor Robo1. While it has not been determined whether Robo1 is a substrate of ADAM17, it is possible that cleavage of Robo1 inhibits its repulsive function, which could explain the reduced commissure formation observed in *Adam17* cKO embryos. One would predict that, as a result, overexpression of Tace or ADAM17 should inhibit Robo1-mediated repulsion, which is contrary to what we observed in *Drosophila* (Figures S2K–S2M). This again argues against Robo1 as the primary substrate mediating the phenotypes observed in *Adam17* cKO embryos.

Regulation of tace and ADAM17 activity

Our data suggest that Tace and ADAM17 are strictly regulated to achieve a precise balance of Fra and Dcc signaling outputs. What are the mechanisms involved in commissural neurons to modulate Tace and ADAM17 expression and/or activity? In principle, this regulation could occur either at the metalloprotease level or at the substrate level. First, the surface expression or the activity of Tace and ADAM17 could be regulated. We have demonstrated that *tace* and *Adam17* transcripts are highly expressed in the embryonic CNS of both invertebrates and vertebrates (Figures 1, 6, and S6). In *Drosophila*, the expression of Tace mRNA and protein does not appear to be temporally controlled, suggesting that Tace activity is likely to be regulated post-translationally. Indeed, a number of molecules have been identified as regulators of ADAM17 activity, including tissue inhibitor of metalloproteinases-3 (TIMP-3) which suppresses ADAM17 catalytic activity,[62] and the adapter proteins iRhom1 and iRhom2, which are involved in ADAM17 maturation and stability.[63] Thus, it would be interesting to explore the potential roles of TIMP-3 and the iRhoms and their *Drosophila* orthologs during axon guidance.

Alternatively, regulation of Tace and ADAM17 function could occur at the substrate level. Ligand binding could induce conformational changes in the substrate to facilitate its association with the metalloprotease, or an interacting protein could bind to the substrate to block association with the metalloprotease. We have demonstrated previously that netrin does not activate the transcriptional activity of Fra,[21] suggesting that an alternative ligand may exist for the non-canonical pathway. In mouse cortical neurons, leucine-rich repeats and immunoglobulin-like

domains 2 (Lrig2) bind to neogenin to inhibit premature ADAM17 cleavage.[55] It remains to be seen whether similar mechanisms regulate Fra and Dcc cleavage.

Tace and ADAM17 coordinate the canonical and non-canonical pathways

ADAMs can facilitate a switch in responses to guidance cues. For example, ADAM10 and ADAM17 cleave Neuropilin-1 to regulate proprioceptive axon responsiveness to Sema3A.[53] In addition, ADAM10 cleaves ephrinA5 to convert EphA3-ephrinA5-mediated adhesion to repulsion.[54] We propose that Tace and ADAM17 can instruct neurons to coordinate the canonical and non-canonical pathways. It is important to point out that, instead of producing opposite signaling outcomes, the canonical and non-canonical pathways both promote midline crossing of commissural axons (Figures 7K and 7L), which suggests that the two pathways cooperate instead of competing. This distinguishes our model from existing mechanisms, but at the same time inevitably poses the question: how does the neuron decide between the two pathways? We speculate that both pathways could be engaged in the same cell but are separated spatially and/or temporally. The canonical pathway is activated at the tip of the axon, where Fra responds to netrin to locally regulate the cytoskeleton.[2] It is possible that the non-canonical Fra pathway is activated in the soma instead, where the cleaved Fra ICDs are within close proximity to the nucleus. This is supported by our observation that both endogenous Tace and overexpressed Tace are almost exclusively detected in the cell soma but not on the axons. In addition, the two pathways could be activated by distinct ligands, so that they are controlled at different developmental time points. Given the diverse roles of ADAM family metalloproteases in development and disease, continued investigation into their regulation and mechanism of action will undoubtedly offer important biological insights.

Limitations of the study

While we demonstrated that Tace/ADAM17 is a key regulator of Fra/Dcc signaling and controls midline axon guidance, this study has its limitations. First, *tace* zygotic mutants in *Drosophila* show midline crossing defects with low penetrance, which is likely the result of a maternal effect. Yet we were unable to definitively test this by generating maternal zygotic *tace* mutants, due to developmental arrest potentially linked to its function in the Notch pathway. Second, it remains to be seen if the same non-canonical signaling mechanism is conserved for Dcc in vertebrate systems. Future transcriptomic studies comparing gene expression levels in controls and *Dcc* cKO embryos or cell lines, or cell lines overexpressing Dcc ICD, could help us resolve its role in transcriptional regulation. Third, it is unclear if Tace/ADAM17 is required cell autonomously in commissural neurons or cell non-autonomously in neighboring cells to cleave Fra/Dcc. Generating commissural neuron-specific cKO animals in the future could provide us with definitive answers. Fourth, the commissure formation deficits observed in *Adam17* mutants are not causatively linked to a lack of Dcc cleavage. Finally, it remains to be determined what the biological stimulus that activates the non-canonical pathway is.

STAR★METHODS

Detailed methods are provided in the online version of this paper and include the following:

- KEY RESOURCES TABLE
- RESOURCE AVAILABILITY
  - Lead contact
  - Materials availability
  - Data and code availability
- EXPERIMENTAL MODEL AND SUBJECT DETAILS
  - Drosophila stocks
  - Mouse strains
  - Explant culture
  - Cell culture
- METHOD DETAILS
  - Molecular biology
  - CRISPR Cas9-mediated mutagenesis
  - Cleavage assays
  - Immunoprecipitation
  - Immunostaining
  - RNA *in situ* hybridization
  - RNA extraction and RT-qPCR
  - Electroporation of mouse embryos and explant outgrowth assay
  - Dye injections in open-book spinal cord preparations
  - Data and software
- QUANTIFICATION AND STATISTICAL ANALYSIS

SUPPLEMENTAL INFORMATION

Supplemental information can be found online at https://doi.org/10.1016/j.celrep.2022.111785.

ACKNOWLEDGMENTS

We thank Dr. Wenqin Luo, Dr. Yuanquan Song, Dr. Kaitlin Laws, and other members of the Bashaw lab and the peer reviewers for their feedback on the manuscript. We thank Dr. Madhavi Gorla and Maya Hale for guidance on sectioning and immunostaining of embryonic mouse spinal cord. We thank Dr. Zachary DeLoughery and Dr. Alexander Jaworski for guidance on the *in vitro* explant experiments. We thank Dr. Qu Deng for guidance on qRT-PCR experiments. We thank Dr. Carl Blobel and Dr. Nathalie Burg for the gift of the *Adam17*$^{flox/flox}$ mouse line, Dr. Frederic Charron for the gift of the pGNET1-Myc plasmid, Dr. Patrick Mehlen for the gift of the pCMV-DCC-Myc plasmid, and Dr. Wenqin Luo, Dr. Hongjun Song, and Dr. Guo-li Ming for sharing their equipment, as well as the ENCODE project, BDSC, DGRC, BDGP, and FlyBase. This research was supported by NSF IOS-1853719 and NIH R35 NS097340 to G.J.B.

AUTHOR CONTRIBUTIONS

Y.Z. designed and performed all the experiments and wrote the paper. K.C. contributed to mouse spinal cord dissections, the explant outgrowth assay, and the DiI dye injection experiment. G.J.B. designed the experiments, wrote the paper, and supervised the project.

DECLARATION OF INTERESTS

The authors declare no competing interests.

INCLUSION AND DIVERSITY

We support inclusive, diverse, and equitable conduct of research.

Received: May 23, 2022
Revised: October 7, 2022
Accepted: November 15, 2022
Published: December 6, 2022

REFERENCES

1. Neuhaus-Follini, A., and Bashaw, G.J. (2015). The intracellular domain of the frazzled/DCC receptor is a transcription factor required for commissural axon guidance. Neuron *87*, 751–763. https://doi.org/10.1016/j.neuron.2015.08.006.
2. Gorla, M., and Bashaw, G.J. (2020). Molecular mechanisms regulating axon responsiveness at the midline. Dev. Biol. *466*, 12–21. https://doi.org/10.1016/j.ydbio.2020.08.006.
3. Engle, E.C. (2010). Human genetic disorders of axon guidance. Cold Spring Harb. Perspect. Biol. *2*, a001784. https://doi.org/10.1101/cshperspect.a001784.
4. Nugent, A.A., Kolpak, A.L., and Engle, E.C. (2012). Human disorders of axon guidance. Curr. Opin. Neurobiol. *22*, 837–843. https://doi.org/10.1016/j.conb.2012.02.006.
5. Van Battum, E.Y., Brignani, S., and Pasterkamp, R.J. (2015). Axon guidance proteins in neurological disorders. Lancet Neurol. *14*, 532–546. https://doi.org/10.1016/s1474-4422(14)70257-1.
6. Srour, M., Rivière, J.B., Pham, J.M.T., Dubé, M.P., Girard, S., Morin, S., Dion, P.A., Asselin, G., Rochefort, D., Hince, P., et al. (2010). Mutations in DCC cause congenital mirror movements. Science *328*, 592. https://doi.org/10.1126/science.1186463.
7. Depienne, C., Cincotta, M., Billot, S., Bouteiller, D., Groppa, S., Brochard, V., Flamand, C., Hubsch, C., Meunier, S., Giovannelli, F., et al. (2011). A novel DCC mutation and genetic heterogeneity in congenital mirror movements. Neurology *76*, 260–264. https://doi.org/10.1212/WNL.0b013e318207b1e0.
8. Jen, J.C., Chan, W.-M., Bosley, T.M., Wan, J., Carr, J.R., Rüb, U., Shattuck, D., Salamon, G., Kudo, L.C., Ou, J., et al. (2004). Mutations in a human ROBO gene disrupt hindbrain axon pathway crossing and morphogenesis. Science *304*, 1509–1513. https://doi.org/10.1126/science.1096437.
9. Hannula-Jouppi, K., Kaminen-Ahola, N., Taipale, M., Eklund, R., Nopola-Hemmi, J., Kääriäinen, H., and Kere, J. (2005). The axon guidance receptor gene ROBO1 is a candidate gene for developmental dyslexia. PLoS Genet. *1*, e50. https://doi.org/10.1371/journal.pgen.0010050.
10. Jamuar, S.S., Schmitz-Abe, K., D'Gama, A.M., Drottar, M., Chan, W.M., Peeva, M., Servattalab, S., Lam, A.T.N., Delgado, M.R., Clegg, N.J., et al. (2017). Biallelic mutations in human DCC cause developmental split-brain syndrome. Nat. Genet. *49*, 606–612. https://doi.org/10.1038/ng.3804.
11. Serafini, T., Kennedy, T.E., Galko, M.J., Mirzayan, C., Jessell, T.M., and Tessier-Lavigne, M. (1994). The netrins define a family of axon outgrowth-promoting proteins homologous to C. elegans UNC-6. Cell *78*, 409–424. https://doi.org/10.1016/0092-8674(94)90420-0.
12. Kennedy, T.E., Serafini, T., de la Torre, J.R., and Tessier-Lavigne, M. (1994). Netrins are diffusible chemotropic factors for commissural axons in the embryonic spinal cord. Cell *78*, 425–435. https://doi.org/10.1016/0092-8674(94)90421-9.
13. Harris, R., Sabatelli, L.M., and Seeger, M.A. (1996). Guidance cues at the Drosophila CNS midline: identification and characterization of two Drosophila netrin/UNC-6 homologs. Neuron *17*, 217–228. https://doi.org/10.1016/s0896-6273(00)80154-3.
14. Keino-Masu, K., Masu, M., Hinck, L., Leonardo, E.D., Chan, S.S., Culotti, J.G., and Tessier-Lavigne, M. (1996). Deleted in colorectal cancer (DCC) encodes a netrin receptor. Cell *87*, 175–185. https://doi.org/10.1016/s0092-8674(00)81336-7.
15. Kolodziej, P.A., Timpe, L.C., Mitchell, K.J., Fried, S.R., Goodman, C.S., Jan, L.Y., and Jan, Y.N. (1996). Frazzled encodes a Drosophila member of the DCC immunoglobulin subfamily and is required for CNS and motor axon guidance. Cell *87*, 197–204. https://doi.org/10.1016/s0092-8674(00)81338-0.
16. Mitchell, K.J., Doyle, J.L., Serafini, T., Kennedy, T.E., Tessier-Lavigne, M., Goodman, C.S., and Dickson, B.J. (1996). Genetic analysis of netrin genes in Drosophila: netrins guide CNS commissural axons and peripheral motor axons. Neuron *17*, 203–215. https://doi.org/10.1016/s0896-6273(00)80153-1.
17. Serafini, T., Colamarino, S.A., Leonardo, E.D., Wang, H., Beddington, R., Skarnes, W.C., and Tessier-Lavigne, M. (1996). Netrin-1 is required for commissural axon guidance in the developing vertebrate nervous system. Cell *87*, 1001–1014. https://doi.org/10.1016/s0092-8674(00)81795-x.
18. Fazeli, A., Dickinson, S.L., Hermiston, M.L., Tighe, R.V., Steen, R.G., Small, C.G., Stoeckli, E.T., Keino-Masu, K., Masu, M., Rayburn, H., et al. (1997). Phenotype of mice lacking functional Deleted in colorectal cancer (Dec) gene. Nature *386*, 796–804. https://doi.org/10.1038/386796a0.
19. Brankatschk, M., and Dickson, B.J. (2006). Netrins guide Drosophila commissural axons at short range. Nat. Neurosci. *9*, 188–194. https://doi.org/10.1038/nn1625.
20. Zang, Y., Chaudhari, K., and Bashaw, G.J. (2021). New insights into the molecular mechanisms of axon guidance receptor regulation and signaling. Curr. Top. Dev. Biol. *142*, 147–196. https://doi.org/10.1016/bs.ctdb.2020.11.008.
21. Yang, L., Garbe, D.S., and Bashaw, G.J. (2009). A frazzled/DCC-dependent transcriptional switch regulates midline axon guidance. Science *324*, 944–947. https://doi.org/10.1126/science.1171320.
22. Keleman, K., Rajagopalan, S., Cleppien, D., Teis, D., Paiha, K., Huber, L.A., Technau, G.M., and Dickson, B.J. (2002). Comm sorts robo to control axon guidance at the Drosophila midline. Cell *110*, 415–427. https://doi.org/10.1016/s0092-8674(02)00901-7.
23. Keleman, K., Ribeiro, C., and Dickson, B.J. (2005). Comm function in commissural axon guidance: cell-autonomous sorting of Robo in vivo. Nat. Neurosci. *8*, 156–163. https://doi.org/10.1038/nn1388.
24. Taniguchi, Y., Kim, S.H., and Sisodia, S.S. (2003). Presenilin-dependent "gamma-secretase" processing of deleted in colorectal cancer (DCC). J. Biol. Chem. *278*, 30425–30428. https://doi.org/10.1074/jbc.C300239200.
25. Goldschneider, D., Rama, N., Guix, C., and Mehlen, P. (2008). The neogenin intracellular domain regulates gene transcription via nuclear translocation. Mol. Cell Biol. *28*, 4068–4079. https://doi.org/10.1128/MCB.02114-07.
26. Brown, M.S., Ye, J., Rawson, R.B., and Goldstein, J.L. (2000). Regulated intramembrane proteolysis. Cell *100*, 391–398. https://doi.org/10.1016/s0092-8674(00)80675-3.
27. Ehrmann, M., and Clausen, T. (2004). Proteolysis as a regulatory mechanism. Annu. Rev. Genet. *38*, 709–724. https://doi.org/10.1146/annurev.genet.38.072902.093416.
28. Lichtenthaler, S.F., Lemberg, M.K., and Fluhrer, R. (2018). Proteolytic ectodomain shedding of membrane proteins in mammals-hardware, concepts, and recent developments. EMBO J. *37*, e99456. https://doi.org/10.15252/embj.201899456.
29. Seals, D.F., and Courtneidge, S.A. (2003). The ADAMs family of metalloproteases: multidomain proteins with multiple functions. Genes Dev. *17*, 7–30. https://doi.org/10.1101/gad.1039703.
30. Edwards, D.R., Handsley, M.M., and Pennington, C.J. (2008). The ADAM metalloproteinases. Mol. Aspects Med. *29*, 258–289. https://doi.org/10.1016/j.mam.2008.08.001.
31. Hsia, H.-E., Tüshaus, J., Brummer, T., Zheng, Y., Scilabra, S.D., and Lichtenthaler, S.F. (2019). Functions of 'A disintegrin and metalloproteases (ADAMs)' in the mammalian nervous system. Cell. Mol. Life Sci. *76*, 3055–3081. https://doi.org/10.1007/s00018-019-03173-7.

32. Galko, M.J., and Tessier-Lavigne, M. (2000). Function of an axonal chemoattractant modulated by metalloprotease activity. Science *289*, 1365–1367. https://doi.org/10.1126/science.289.5483.1365.

33. Odden, J.P., Holbrook, S., and Doe, C.Q. (2002). DrosophilaHB9Is expressed in a subset of motoneurons and interneurons, where it regulates gene expression and axon pathfinding. J. Neurosci. *22*, 9143–9149. https://doi.org/10.1523/jneurosci.22-21-09143.2002.

34. Dittrich, R., Bossing, T., Gould, A.P., Technau, G.M., and Urban, J. (1997). The differentiation of the serotonergic neurons in the Drosophila ventral nerve cord depends on the combined function of the zinc finger proteins Eagle and Huckebein. Development *124*, 2515–2525. https://doi.org/10.1242/dev.124.13.2515.

35. Garbe, D.S., O'Donnell, M., and Bashaw, G.J. (2007). Cytoplasmic domain requirements for Frazzled-mediated attractive axon turning at the Drosophila midline. Development *134*, 4325–4334. https://doi.org/10.1242/dev.012872.

36. Yang, L., and Bashaw, G.J. (2006). Son of sevenless directly links the robo receptor to rac activation to control axon repulsion at the midline. Neuron *52*, 595–607. https://doi.org/10.1016/j.neuron.2006.09.039.

37. Chaudhari, K., Gorla, M., Chang, C., Kania, A., and Bashaw, G.J. (2021). Robo recruitment of the Wave regulatory complex plays an essential and conserved role in midline repulsion. Elife *10*, e64474. https://doi.org/10.7554/eLife.64474.

38. Coleman, H.A., Labrador, J.P., Chance, R.K., and Bashaw, G.J. (2010). The Adam family metalloprotease Kuzbanian regulates the cleavage of the roundabout receptor to control axon repulsion at the midline. Development *137*, 2417–2426. https://doi.org/10.1242/dev.047993.

39. Chance, R.K., and Bashaw, G.J. (2015). Slit-dependent endocytic trafficking of the robo receptor is required for son of sevenless recruitment and midline axon repulsion. PLoS Genet. *11*, e1005402. https://doi.org/10.1371/journal.pgen.1005402.

40. Brown, J.B., Boley, N., Eisman, R., May, G.E., Stoiber, M.H., Duff, M.O., Booth, B.W., Wen, J., Park, S., Suzuki, A.M., et al. (2014). Diversity and dynamics of the Drosophila transcriptome. Nature *512*, 393–399. https://doi.org/10.1038/nature12962.

41. Solomon, K.A., Pesti, N., Wu, G., and Newton, R.C. (1999). Cutting edge: a dominant negative form of TNF-alpha converting enzyme inhibits proTNF and TNFRII secretion. J. Immunol. *163*, 4105–4108.

42. Wolfe, M.S. (2019). Structure and function of the gamma-secretase complex. Biochemistry *58*, 2953–2966. https://doi.org/10.1021/acs.biochem.9b00401.

43. Nagarkar-Jaiswal, S., Lee, P.T., Campbell, M.E., Chen, K., Anguiano-Zarate, S., Cantu Gutierrez, M., Busby, T., Lin, W.W., He, Y., Schulze, K.L., et al. (2015). A library of MiMICs allows tagging of genes and reversible, spatial and temporal knockdown of proteins in Drosophila. Elife *4*. https://doi.org/10.7554/eLife.05338.

44. Santiago, C., and Bashaw, G.J. (2017). Islet coordinately regulates motor axon guidance and dendrite targeting through the frazzled/DCC receptor. Cell Rep. *18*, 1646–1659. https://doi.org/10.1016/j.celrep.2017.01.041.

45. Uhlén, M., Fagerberg, L., Hallström, B.M., Lindskog, C., Oksvold, P., Mardinoglu, A., Sivertsson, Å., Kampf, C., Sjöstedt, E., Asplund, A., et al. (2015). Proteomics. Tissue-based map of the human proteome. Science *347*, 1260419. https://doi.org/10.1126/science.1260419.

46. Sahin, U., Weskamp, G., Kelly, K., Zhou, H.M., Higashiyama, S., Peschon, J., Hartmann, D., Saftig, P., and Blobel, C.P. (2004). Distinct roles for ADAM10 and ADAM17 in ectodomain shedding of six EGFR ligands. J. Cell Biol. *164*, 769–779. https://doi.org/10.1083/jcb.200307137.

47. Ludwig, A., Hundhausen, C., Lambert, M.H., Broadway, N., Andrews, R.C., Bickett, D.M., Leesnitzer, M.A., and Becherer, J.D. (2005). Metalloproteinase inhibitors for the disintegrin-like metalloproteinases ADAM10 and ADAM17 that differentially block constitutive and phorbol ester-inducible shedding of cell surface molecules. Comb. Chem. High Throughput Screen. *8*, 161–171. https://doi.org/10.2174/1386207053258488.

48. Gorla, M., Santiago, C., Chaudhari, K., Layman, A.A.K., Oliver, P.M., and Bashaw, G.J. (2019). Ndfip proteins target robo receptors for degradation and allow commissural axons to cross the midline in the developing spinal cord. Cell Rep. *26*, 3298–3312.e4, e3294. https://doi.org/10.1016/j.celrep.2019.02.080.

49. Tronche, F., Kellendonk, C., Kretz, O., Gass, P., Anlag, K., Orban, P.C., Bock, R., Klein, R., and Schütz, G. (1999). Disruption of the glucocorticoid receptor gene in the nervous system results in reduced anxiety. Nat. Genet. *23*, 99–103. https://doi.org/10.1038/12703.

50. Moreno-Bravo, J.A., Roig Puiggros, S., Mehlen, P., and Chédotal, A. (2019). Synergistic activity of floor-plate- and ventricular-zone-derived netrin-1 in spinal cord commissural axon guidance. Neuron *101*, 625–634.e3, e623. https://doi.org/10.1016/j.neuron.2018.12.024.

51. Tulloch, A.J., Teo, S., Carvajal, B.V., Tessier-Lavigne, M., and Jaworski, A. (2019). Diverse spinal commissural neuron populations revealed by fate mapping and molecular profiling using a novelRobo3Cremouse. J. Comp. Neurol. *527*, 2948–2972. https://doi.org/10.1002/cne.24720.

52. Charron, F., Stein, E., Jeong, J., McMahon, A.P., and Tessier-Lavigne, M. (2003). The morphogen sonic hedgehog is an axonal chemoattractant that collaborates with netrin-1 in midline axon guidance. Cell *113*, 11–23. https://doi.org/10.1016/s0092-8674(03)00199-5.

53. Romi, E., Gokhman, I., Wong, E., Antonovsky, N., Ludwig, A., Sagi, I., Saftig, P., Tessier-Lavigne, M., and Yaron, A. (2014). ADAM metalloproteases promote a developmental switch in responsiveness to the axonal repellant Sema3A. Nat. Commun. *5*, 4058. https://doi.org/10.1038/ncomms5058.

54. Janes, P.W., Saha, N., Barton, W.A., Kolev, M.V., Wimmer-Kleikamp, S.H., Nievergall, E., Blobel, C.P., Himanen, J.P., Lackmann, M., and Nikolov, D.B. (2005). Adam meets Eph: an ADAM substrate recognition module acts as a molecular switch for ephrin cleavage in trans. Cell *123*, 291–304. https://doi.org/10.1016/j.cell.2005.08.014.

55. van Erp, S., van den Heuvel, D.M.A., Fujita, Y., Robinson, R.A., Hellemons, A.J.C.G.M., Adolfs, Y., Van Battum, E.Y., Blokhuis, A.M., Kuijpers, M., Demmers, J.A.A., et al. (2015). Lrig2 negatively regulates ectodomain shedding of axon guidance receptors by ADAM proteases. Dev. Cell *35*, 537–552. https://doi.org/10.1016/j.devcel.2015.11.008.

56. Bai, G., Chivatakarn, O., Bonanomi, D., Lettieri, K., Franco, L., Xia, C., Stein, E., Ma, L., Lewcock, J.W., and Pfaff, S.L. (2011). Presenilin-dependent receptor processing is required for axon guidance. Cell *144*, 106–118. https://doi.org/10.1016/j.cell.2010.11.053.

57. Okamura, Y., Kohmura, E., and Yamashita, T. (2011). TACE cleaves neogenin to desensitize cortical neurons to the repulsive guidance molecule. Neurosci. Res. *71*, 63–70. https://doi.org/10.1016/j.neures.2011.05.012.

58. Banerjee, P., Harada, H., Tassew, N.G., Charish, J., Goldschneider, D., Wallace, V.A., Sugita, S., Mehlen, P., and Monnier, P.P. (2016). Upsilon-secretase and LARG mediate distinct RGMa activities to control appropriate layer targeting within the optic tectum. Cell Death Differ. *23*, 442–453. https://doi.org/10.1038/cdd.2015.111.

59. Brown, S., Jayachandran, P., Negesse, M., Olmo, V., Vital, E., and Brewster, R. (2019). Rgma-induced Neo1 proteolysis promotes neural tube morphogenesis. J. Neurosci. *39*, 7465–7484. https://doi.org/10.1523/JNEUROSCI.3262-18.2019.

60. Neuhaus-Follini, A., and Bashaw, G.J. (2015). Crossing the Embryonic Midline: Molecular Mechanisms Regulating Axon Responsiveness at an Intermediate Target, *4* (Wiley Interdiscip Rev Dev Biol), pp. 377–389. https://doi.org/10.1002/wdev.185.

61. Xu, K., Wu, Z., Renier, N., Antipenko, A., Tzvetkova-Robev, D., Xu, Y., Minchenko, M., Nardi-Dei, V., Rajashankar, K.R., Himanen, J., et al. (2014). Structures of netrin-1 bound to two receptors provide insight into its axon guidance mechanism. Science *344*, 1275–1279. https://doi.org/10.1126/science.1255149.

62. Brew, K., and Nagase, H. (2010). The tissue inhibitors of metalloproteinases (TIMPs): an ancient family with structural and functional diversity. Biochim. Biophys. Acta *1803*, 55–71. https://doi.org/10.1016/j.bbamcr.2010.01.003.

63. Düsterhöft, S., Babendreyer, A., Giese, A.A., Flasshove, C., and Ludwig, A. (2019). Status update on iRhom and ADAM17: it's still complicated. Biochim. Biophys. Acta. Mol. Cell Res. *1866*, 1567–1583. https://doi.org/10.1016/j.bbamcr.2019.06.017.

64. Horiuchi, K., Kimura, T., Miyamoto, T., Takaishi, H., Okada, Y., Toyama, Y., and Blobel, C.P. (2007). Cutting edge: TNF-α-Converting enzyme (TACE/ADAM17) inactivation in mouse myeloid cells prevents lethality from endotoxin shock. J. Immunol. *179*, 2686–2689. https://doi.org/10.4049/jimmunol.179.5.2686.

65. Lukinova, N.I., Roussakova, V.V., and Fortini, M.E. (1999). Genetic characterization of cytological region 77A–D harboring the presenilin gene of Drosophila melanogaster. Genetics *153*, 1789–1797. https://doi.org/10.1093/genetics/153.4.1789.

66. Kidd, T., Brose, K., Mitchell, K.J., Fetter, R.D., Tessier-Lavigne, M., Goodman, C.S., and Tear, G. (1998). Roundabout controls axon crossing of the CNS midline and defines a novel subfamily of evolutionarily conserved guidance receptors. Cell *92*, 205–215. https://doi.org/10.1016/s0092-8674(00)80915-0.

67. Nüsslein-Volhard, C., Wieschaus, E., and Kluding, H. (1984). Mutations affecting the pattern of the larval cuticle inDrosophila melanogaster. Wilehm. Roux. Arch. Dev. Biol. *193*, 267–282. https://doi.org/10.1007/bf00848156.

68. Sotillos, S., Roch, F., and Campuzano, S. (1997). The metalloprotease-disintegrin Kuzbanian participates in Notch activation during growth and patterning of Drosophila imaginal discs. Development *124*, 4769–4779. https://doi.org/10.1242/dev.124.23.4769.

69. Luo, L., Liao, Y.J., Jan, L.Y., and Jan, Y.N. (1994). Distinct morphogenetic functions of similar small GTPases: Drosophila Drac1 is involved in axonal outgrowth and myoblast fusion. Genes Dev. *8*, 1787–1802. https://doi.org/10.1101/gad.8.15.1787.

70. Benveniste, R.J., Thor, S., Thomas, J.B., and Taghert, P.H. (1998). Cell type-specific regulation of the Drosophila FMRF-NH2 neuropeptide gene by Apterous, a LIM homeodomain transcription factor. Development *125*, 4757–4765.

71. Li-Kroeger, D., Kanca, O., Lee, P.-T., Cowan, S., Lee, M.T., Jaiswal, M., Salazar, J.L., He, Y., Zuo, Z., and Bellen, H.J. (2018). An expanded toolkit for gene tagging based on MiMIC and scarless CRISPR tagging in Drosophila. Elife *7*, e38709. https://doi.org/10.7554/eLife.38709.

72. O'Donnell, M.P., and Bashaw, G.J. (2013). Src inhibits midline axon crossing independent of frazzled/deleted in colorectal carcinoma (DCC) receptor tyrosine phosphorylation. J. Neurosci. *33*, 305–314. https://doi.org/10.1523/jneurosci.2756-12.2013.

73. Port, F., Chen, H.M., Lee, T., and Bullock, S.L. (2014). Optimized CRISPR/Cas tools for efficient germline and somatic genome engineering in Drosophila. Proc. Natl. Acad. Sci. USA *111*, E2967–E2976. https://doi.org/10.1073/pnas.1405500111.

74. Zirin, J., Hu, Y., Liu, L., Yang-Zhou, D., Colbeth, R., Yan, D., Ewen-Campen, B., Tao, R., Vogt, E., VanNest, S., et al. (2020). Large-scale transgenic Drosophila resource collections for loss- and gain-of-function studies. Genetics *214*, 755–767. https://doi.org/10.1534/genetics.119.302964.

75. Bashaw, G.J. (2010). Visualizing axons in the Drosophila central nervous system using immunohistochemistry and immunofluorescence. Cold Spring Harb. Protoc. *2010*, pdb.prot5503. https://doi.org/10.1101/pdb.prot5503.

76. Labrador, J.P., O'Keefe, D., Yoshikawa, S., McKinnon, R.D., Thomas, J.B., and Bashaw, G.J. (2005). The homeobox transcription factor even-skipped regulates netrin-receptor expression to control dorsal motor-axon projections in Drosophila. Curr. Biol. *15*, 1413–1419. https://doi.org/10.1016/j.cub.2005.06.058.

77. Fleming, M.S., Ramos, D., Han, S.B., Zhao, J., Son, Y.-J., and Luo, W. (2012). The majority of dorsal spinal cord gastrin releasing peptide is synthesized locally whereas neuromedin B is highly expressed in pain- and itch-sensing Somatosensory neurons. Mol. Pain *8*, 52. https://doi.org/10.1186/1744-8069-8-52.

78. Luo, L., Ambrozkiewicz, M.C., Benseler, F., Chen, C., Dumontier, E., Falkner, S., Furlanis, E., Gomez, A.M., Hoshina, N., Huang, W.-H., et al. (2020). Optimizing nervous system-specific gene targeting with cre driver lines: Prevalence of germline recombination and Influencing factors. Neuron *106*, 37–65.e5. https://doi.org/10.1016/j.neuron.2020.01.008.

STAR★METHODS

KEY RESOURCES TABLE

REAGENT or RESOURCE	SOURCE	IDENTIFIER
Antibodies		
Mouse anti-Myc, 1:1000 (WB)	DSHB	Cat#9E10-C
Rabbit anti-Myc, 1:500 (IF)	Sigma-Aldrich	Cat#C3956
Rabbit anti-Myc, 1.5 μg (IP)	Millipore	Cat#06-549
Mouse anti-HA, 1:500 (IF), 1:1000 (WB), 1.5 μg (IP)	BioLegend	Cat#901502
Mouse anti-beta tubulin, 1:300 (IF), 1:1000 (WB)	DSHB	Cat#E7-S
Chick anti-beta gal, 1:500 (IF)	Abcam	Cat#ab9361
Mouse anti-Fasciclin II, 1:50 (IF)	DSHB	Cat#1D4
Rabbit anti-GFP, 1:300 (IF)	Invitrogen	Cat#a11122
Rabbit anti-dsRed, 1:200 (IF)	Takara	Cat#632496
Mouse anti-Scar (supernatant), 1:50 (IF)	DSHB	Cat#P1C1
Mouse anti-Slit (supernatant), 1:100 (IF)	DSHB	Cat#C555.6D
Mouse anti-Elav (supernatant), 1:20 (IF)	DSHB	Cat#9F8A9
Mouse anti-Repo (supernatant), 1:20 (IF)	DSHB	Cat#8D12
Mouse anti-Islet (supernatant), 1:20 (IF)	DSHB	Cat#40.3A4
Mouse anti-Sex lethal (supernatant), 1:20 (IF)	DSHB	Cat#M114
Goat anti-Robo3, 1:200 (IHC)	R & D systems	Cat#AF3076
Mouse anti-Dcc, 1:1000 (WB)	BD Biosciences	Cat#554223
Mouse anti-Brn-3a, 1:200 (IF)	Chemicon	Cat#MAB1585
Mouse anti-Lhx1/5, 1:200 (IF)	DSHB	Cat#4F2
Rabbit anti-Cleaved Caspase-3, 1:1000 (IF)	Cell Signaling	Cat#9664
Sheep anti-DIG-POD antibody, 1:60 (RNA FISH)	Roche	Cat#11207733910
Sheep Anti-Digoxigenin-AP, Fab fragments, 1:1000 (RNA FISH)	Roche	Cat#11093274910
Alexa647 Goat anti-HRP, 1:500 (IF)	Jackson Immnuoresearch	Cat#123-605-021
Goat anti-Mouse HRP, 1:10,000 (WB)	Jackson Immnuoresearch	Cat#115-035-146
Goat anti-Rabbit HRP, 1:10,000 (WB)	Jackson Immnuoresearch	Cat#111-035-003
Cy3 Donkey anti-Goat, 1:500 (IF)	Jackson Immnuoresearch	Cat#705-165-147
Alexa488 Goat anti-Rabbit, 1:500 (IF)	Invitrogen	Cat#A11034
Alexa488 Goat anti-Mouse, 1:500 (IF)	Invitrogen	Cat#A11029
Alexa488 Goat anti-Chick, 1:500 (IF)	Invitrogen	Cat#A11039
Cy3 Goat anti-Mouse, 1:500 (IF)	Jackson Immnuoresearch	Cat#115-165-003
Cy3 Goat anti-Rabbit, 1:500 (IF)	Jackson Immnuoresearch	Cat#111-165-003
Cy3 Goat anti-Chick, 1:500 (IF)	Abcam	Cat#ab97145
Chemicals, peptides, and recombinant proteins		
DMEM	Invitrogen	Cat#11965084
Horse serum	Gibco	Cat#16050122
Fetal bovine serum	Gibco	Cat#10437-028
Normal goat serum	Gibco	Cat#16210-064
Opti-MEM	Gibco	Cat#31985-070
F12	Gibco	Cat#11765-054
Glucose	Thermo Fisher	Cat#D16-500
100x Pen/Strep/Glutamine	Gibco	Cat#10378-016
HBSS	Gibco	Cat#14175-079
Trypsin	Gibco	Cat#25300054
Neurobasal	Gibco	Cat#21103-049

(*Continued on next page*)

Continued

REAGENT or RESOURCE	SOURCE	IDENTIFIER
FBS	Gibco	Cat#10437-028
B-27	ThermoFisher	Cat#A3582801
Effectene Transfection Reagent	Qiagen	Cat#301425
Direct PCR Lysis Reagent (Mouse Tail)	Viagen Biotech	Cat#101-T
KAPA2G HotStart ReadyMix with dye	Roche	Cat#KK5609
RNeasy Plus Mini Kit	Qiagen	Cat#74134
SuperScriptIV	Life Technologies	Cat#18090200
Fast SYBR Master Mix	Life Technologies	Cat#4385617
Rat Tail Collagen	Corning	Cat#354249
Paraformaldehyde 16% Solution, EM grade	Electron Microscopy Services	Cat#15710
Epredia Aqua-Mount Slide Mounting Media	Epredia	Cat#13800
Epredia Neg-50 Frozen Section Medium	Epredia	Cat# 6502
Phorbol 12-myristate 13-acetate, PMA	Sigma-Aldrich	Cat#P8139
GM6001	Millipore	Cat#364205-1MG
TAPI-1	Sigma-Aldrich	Cat#579053-500UG
GI254023X	Sigma-Aldrich	Cat#SML0789-5MG
GM1489	Calbiochem	Cat#364200
Formamide (Molecular Biology)	Fisher BioReagents	Cat#BP227500
Denhardt's Solution 50x	Sigma-Aldrich	Cat# D2532
Salmon Sperm DNA	Stratagene	Cat#201190
tRNA	Roche	Cat#10109541001
Heparin	Sigma-Aldrich	Cat#H4784
SSC, 20X	Invitrogen	Cat#15557036
Dextran Sulfate	Fisher BioReagents	Cat# BP1585100
Tween-20	Bio-Rad	Cat#1706531
Triton X-100	Sigma-Aldrich	Cat#T8787-100ML
TSA fluorescein system	AKOYA	Cat#NEL701A001KT
Recombinant Mouse Netrin-1 Protein	R & D systems	Cat#1109-N1-025
Schneider's Drosophila Medium	Life Technologies	Cat#21720024
Surfact-AMPS NP40	ThermoFisher	Cat#85124
Sodium orthovanadate	Sigma-Aldrich	Cat#S6508
Protease Inhibitor (Complete)	Roche	Cat#11697498001
2x Laemmli Sample Buffer	Bio-Rad	Cat#1610737
4x Laemmli Sample Buffer	Bio-Rad	Cat#1610747
BME (2-mercaptoethanol)	Bio-Rad	Cat#1610710
Clarity Western ECL Substrate	Bio-Rad	Cat#1705061
Essendant Liquid Bleach	Essendant	Cat#KIKBLEACH6
*Not*I	New England Biolabs	Cat#R3189S
*Xba*I	New England Biolabs	Cat#R0145S
EagI	New England Biolabs	Cat#R3505S
*Xho*I	New England Biolabs	Cat#R0146S
*Bbs*I	New England Biolabs	Cat#R3539S
AseI	New England Biolabs	Cat#R0526S
DpnI	New England Biolabs	Cat#R0176S
T7 RNA Polymerase	Promega Corp.	Cat#P2075
10x DIG labeled-NTP	Roche	Cat#11277073910
DNAse	Roche	Cat#776785
Protein A Agarose beads	Invitrogen	Cat#15918-014
rProteinG Agarose beads	Invitrogen	Cat#15920-010
Nitro blue tetrazolium (NBT)	Roche	Cat#11383213001

(*Continued on next page*)

Continued

REAGENT or RESOURCE	SOURCE	IDENTIFIER
5-bromo-4-chloro-3-indolyl-phosphate (BCIP)	Roche	Cat#1138221001
DiI	Sigma Aldrich	Cat#468495-100MG
Experimental models: Cell lines		
293T	ATCC	Cat#ATCC CRL-3216
S2R+	Drosophila Genomics Resource Center	Cat#150
Experimental models: Organisms/strains		
Mouse: CD-1	Charles River	Stock#022
Mouse: B6.Cg-Tg(Nes-cre)1Kln/J	The Jackson Laboratory	Stock#003771
Mouse: *Adam17*$^{flox/flox}$	Horiuchi et al., 2007[64]	N/A
D. melanogaster: w^{1118}	Bloomington Drosophila Stock Center	Stock#3605
D. melanogaster: $tace^{19}$	This study	N/A
D. melanogaster: $tace^{17}$	This study	N/A
D. melanogaster: $tace^{DF}$	Bloomington Drosophila Stock Center	Stock#27366
D. melanogaster: *tace-EGFP*	This study	N/A
D. melanogaster: fra^{3}	Kolodziej et al.[15]	N/A
D. melanogaster: fra^{4}	Kolodziej et al.[15]	N/A
D. melanogaster: fra^{6}	Yang et al.[21]	N/A
D. melanogaster: $comm^{e39}$	Yang et al.[21]	N/A
D. melanogaster: psn^{12}	Lukinova et al.[65]	N/A
D. melanogaster: $netAB^{4}$	Brankatschk and Dickson[19]	N/A
D. melanogaster: $robo^{GA285}$	Kidd et al.[66]	N/A
D. melanogaster: $slit^{2}$	Nusslein-Volhard et al.[67]	N/A
D. melanogaster: kuz^{H143}	Sotillos et al.[68]	N/A
D. melanogaster: *eg-Gal4*	Dittrich et al.[34]	N/A
D. melanogaster: *Tl{CRIMIC.TG4.1}Tace*$^{CR02267\text{-}TG4.1}$	Bloomington Drosophila Stock Center	Stock#91497
D. melanogaster: *elav-Gal4*	Luo et al.[69]	N/A
D. melanogaster: *ap-Gal4*	Benveniste et al.[70]	N/A
D. melanogaster: *P{UAS-cd8-GFP}*	Chaudhari et al.[37]	N/A
D. melanogaster: *P{UAS-tau-Myc-GFP}*	Chaudhari et al.[37]	N/A
D. melanogaster: *P{UAS-FraΔC-HA}III*	Garbe et al.[35]	N/A
D. melanogaster: *P{10UAS-HA-Tace}86Fb*	This study	N/A
D. melanogaster: *P{10UAS-HA-Tace}51C*	This study	N/A
D. melanogaster: *P{5UAS-Fra-Myc}III*	Garbe et al.[35]	N/A
D. melanogaster: *P{10UAS-Fra-Myc}86Fb*	Neuhaus-Follini and Bashaw[1]	N/A
D. melanogaster: *P{nos-Cas9.R}*	Bloomington Drosophila Stock Center	Stock#78782
D. melanogaster: *P{TKO.GS01786}*	Bloomington Drosophila Stock Center	Stock#79840
D. melanogaster: *Mi{PT-GFSTF.1}fra*$^{MI06684\text{-}GFSTF.1}$	Bloomington Drosophila Stock Center	Stock#59835
Oligonucleotides		
GCATGAGCGGCCGCACTGCAAAAGACGCTGCGCCA	This study	tace_NotI_fwd
CCATGATCTAGACTAATTACAGGCTCGGGCCAC	This study	tace_XbaI_rev
CCCCATTAATTCTATCATACCCCGTGTGTC	This study	wg_AseI_fwd
TATCGGCCGtAGCGTAATCTGGAACGTCAT	This study	wg_EagI_rev
CTGTCGGCCGTATGCTTTTCAGAGCCCGAAGA	This study	taceΔMP_EagI_fwd
TATATAGGAAAGATATCCGGGTGAACTTCGCAATTC TCGACGAAAAGGCGTTTTAGAGCTAGAAATAGCAAG	This study	tace_CRISPR_fwd
ATTTTAACTTGCTATTTCTAGCTCTAAAACCCGAAAT CTTCTGGCGTGGCGACGTTAAATTGAAAATAGGTC	This study	tace_CRISPR_rev
ACGGGGTGGATAACAAACTGG	This study	tace_genotyping_fwd
TCATTCTGTGTTGCGTATGTTCAA	This study	tace_genotyping_rev

(*Continued on next page*)

Continued

REAGENT or RESOURCE	SOURCE	IDENTIFIER
CACCCGACCCGAATAGAAGC	This study	tace_genotyping_rev2
CCATGATCTAGACTAATTACAGGCTCGG GCCAC TAATACGACTCACTATAG	This study	tace_insitu_rev
AGCCCCGTCACTTTTCGTGTAG	This study	taceCRIMIC_fwd
TGGTGGAGGTACAGGAGAACCAT	This study	taceCRIMIC_rev
CTGTAGCGGCACTCCCAGTTGTTC	Li-Kroeger et al.[71]	T2AGal4_DH_rev
GCACCACGCCGGTGAACAG	Li-Kroeger et al.[71]	GFP_DH_fwd
CATCCGCGACTTGAGAAGCT	This study	ADAM17_qPCR_fwd
TGTCGCAGACTGTAGATCCC	This study	ADAM17_qPCR_rev
CGACTTCAACAGCAACTCCCACTCTTCC	Kindly provided by Dr. Qu Deng	GAPDH _qPCR_fwd
TGGGTGGTCCAGGGTTTCTTACTCCTT	Kindly provided by Dr. Qu Deng	GAPDH _qPCR_rev.
TTGCTAAAGCGCTACATAGGA	The Jackson Laboratory	nestin_wt_fwd
GCCTTATTGTGGAAGGACTG	The Jackson Laboratory	nestin_rev
CCTTCCTGAAGCAGTAGAGCA	The Jackson Laboratory	nestin_tg_fwd
ATGTTCCCCCAGCTAGATTGTTTGCC	Kindly provided by Dr. Nathalie Burg	adam17_flox_1
TACTGGTGGGGAGGGAGAGATTACGAAGGC	Kindly provided by Dr. Nathalie Burg	adam17_flox_2
AATGTGGGGGTGGGTTTTGTT	This study	adam17_wt_fwd
CCCCAGTCCATGCTTAGGTC	This study	adam17_KO_fwd
GACTTCTATGGACCACCCCAC	This study	adam17_KO_rev
AGAGAGCCATCTGAAGAGTTTGT	This study	adam17_insitu_fwd
TAATACGACTCACTATAGTATTCTCGTGGTCACCGCTC	This study	adam17_insitu_rev
Recombinant DNA		
Plasmid: RE65757	Drosophila Genomics Resource Center	Stock#18694
Plasmid: pCFD4: U6:1-gRNA U6:3-gRNA	Addgene	Stock#49411
Plasmid: p10UAST	Neuhaus-Follini and Bashaw[1]	N/A
Plasmid: p10UAST-3xHA-Fra	Neuhaus-Follini and Bashaw[1]	N/A
Plasmid: p10UAST-Fra-6xMyc	Neuhaus-Follini and Bashaw[1]	N/A
Plasmid: p10UAST-3xHA-Tace	This study	N/A
Plasmid: p10UAST-3xHA-TaceΔMP	This study	N/A
Plasmid: pcDNA3-ADAM17-HA	Addgene	Stock#65105
Plasmid: pGNET1-Myc	Kind gift from Dr. Frederic Charron	N/A
Plasmid: pCAG	Chaudhari et al.[37]	N/A
Plasmid: pCAG-ADAM17-HA	This study	N/A
Plasmid: pCAG-RFP	Chaudhari et al.[37]	N/A
Plasmid: pMT-Gal4	Chaudhari et al.[37]	N/A
Plasmid: p10UAST-Dcc-6xMyc	O'Donnell and Bashaw[72]	N/A
Plasmid: pCMV-hDcc-Myc	Kind gift from Dr. Patrick Mehlen	N/A
pcDNA3.1-mADAM17	Addgene	Stock#19141
Equipment, software and algorithms		
FIJI Image J	NIH	https://ImageJ.net/Fiji
Adobe Illustrator	Adobe	N/A
GraphPad Prism 9	GraphPad software	https://www.graphpad.com/
Volocity Software	Perkin Elmer	http://cellularimaging.perkinelmer.com/downloads/
Zen Lite	Carl Zeiss	https://www.zeiss.com/microscopy/us/products/microscope-software/zen-lite.html
Leica Application Suite V3	Leica	https://www.leica-microsystems.com/products/microscope-software/p/leica-application-suite/

(*Continued on next page*)

Continued

REAGENT or RESOURCE	SOURCE	IDENTIFIER
Kimble Kontes Dounce Tissue Grinders, 7ml	DWK Life Sciences	Cat#K885300-0007
QuantStudio3	Applied Biosystems	N/A
Nikon Ti-U microscope	Nikon	N/A
Zeiss LSM 800 microscope	Carl Zeiss	N/A
Leica DM5000B microscope	Leica	N/A
Mini-PROTEAN Tetra Cell	Bio-Rad	Cat#1658034
ChemiDoc Imaging System	Bio-Rad	Cat#171001401

RESOURCE AVAILABILITY

Lead contact

Further information and requests for resources and reagents should be directed to the lead contact, Greg J. Bashaw (gbashaw@pennmedicine.upenn.edu).

Materials availability

Reasonable requests for plasmids and *Drosophila* lines generated by this study, additional resources and additional information should be directed to and will be fulfilled by the lead contact.

Data and code availability

- All data are available in the main text or supplementary materials.
- This paper does not report original code.
- Any additional information required to reanalyze the data reported in this paper is available from the lead contact upon request.

EXPERIMENTAL MODEL AND SUBJECT DETAILS

Drosophila stocks

The following *Drosophila* mutant alleles were used in this study: *tace*^{19}, *tace*^{17}, *tace*^{DF}, *fra*^{3}, *fra*^{4}, *fra*^{6}, *comm*^{e39}, *psn*^{12}, *netAB*$^{\Delta}$, *slit*^{2}, *robo*^{GA285}, *kuz*^{H143}. The following Gal4 lines were used in this study: *eg-Gal4, tace-CRIMIC-Gal4, ap-Gal4, elav-Gal4.* The following transgenic lines were used in this study: *P{UAS-cd8-GFP}, P{UAS-tau-Myc-GFP}, P{UAS-FraΔC-HA}, P{10UAS-HA-Tace}, P{10UAS-Fra-Myc}, P{5UAS-Fra-Myc}, P{nos-Cas9}, P{TKO.GS01786}.* The following endogenously tagged line is used: *Mi{PT-GFSTF.1} fra*$^{MI06684\text{-}GFSTF.1}$, *tace-EGFP.*

The *P{10UAS-HA-Tace}* transgenic flies were generated by BestGene Inc. (Chino Hills, CA) using the PhiC31 integrase-mediated transgenesis system, which generates site-specific integration of transgene into landing sites at cytological positions 86F8 or 51C1. The *tace*^{19} line was generated by cloning two guide RNAs (gRNAs) targeting the first and last exons of *tace* into a pCFD4:U6:1-gRNA U6:3-gRNA vector backbone (Addgene) and sending positive clones to BestGene Inc. (Chino Hills, CA) for injection. Flies were screened by direct sequencing.

The *tace-EGFP* line was generated from the *TI{CRIMIC.TG4.1}Tace*$^{CR02267\text{-}TG4.1}$ line using the Double-Header method detailed in Li-Kroeger et al., 2018. Recombinase Mediated Cassette Exchange (RMCE) events mediated by the PhiC31 integrase were screened using 4 PCR reactions, using the taceCRIMIC_fwd, taceCRIMIC_rev, T2AGal4_DH_rev and GFP_DH_fwd primers.

All crosses were carried out at 25 °C.

Mouse strains

All animal work was approved by the Institutional Animal Care and Use Committee (IACUC) of the University of Pennsylvania. For explant culture assays, embryos were derived from timed pregnant female CD-1 mice that were purchased from Charles River. For RT-qPCR analysis of *Adam17* expression and analysis of commissure thickness, embryos were derived from timed breeding between *Nestin:cre;Adam17*$^{flox/+}$ and *Adam17*$^{flox/flox}$ mice. The *Nestin:cre* line (B6.Cg-Tg(Nes-cre)1Kln/J) was obtained from the Jackson Laboratory.[49] The *Adam17*$^{flox/flox}$ line was kindly provided by Dr. Carl Blobel and Dr. Nathalie Burg.[64] In this study, we counted the day the vaginal plug was found as embryonic day 0.5 (E0.5). Tissues from both male and female embryos (not determined) were used.

Genotypes were determined by PCR using genomic DNA extracted from embryonic tail with Direct PCR Lysis Reagent (Viagen Biotech) and amplified with KAPA2G HotStart ReadyMix (Roche). The following primers was used: 1) nestin_wt_fwd, nestin_rev, nestin_tg_fwd for Cre PCR; 2) adam17_flox_1, adam17_flox_2 for flox PCR; 3) adam17_wt_fwd, adam17_KO_fwd, adam17_KO_rev for

KO PCR. The adam17_KO_fwd, adam17_KO_rev primer set flanks the two *loxP* sites, and successful amplification of a shorter DNA fragment corresponding to the KO allele demonstrates that Cre-mediated recombination events occurred to modify the genomic DNA of cKO embryos (Figures S6A and S6B).

Explant culture

Dorsal spinal cord explants from E12.5 embryos were prepared and cultured in collagen gels.[11] Briefly, E12.5 dorsal spinal cords were isolated, and the dorsal strips were dissected and cut into individual explants. Explants were placed on top of a thin layer of collagen gel, either arranged around a short strip of collagen-embedded 293T cell aggregate or randomly distributed if cultured with recombinant netrin, and sealed with an additional layer of collagen gel on top. Explants were cultured in 50% Opti-MEM (Gibco) and 45% Ham's F-12 media (Gibco) supplemented with 5% horse-serum (Gibco), 0.75% glucose (Thermo Fisher) and 1X penicillin/streptomycin/glutamine (Gibco). Explants were maintained at 5% CO_2 in a 37 °C humidified incubator for approximately 18-24 hours before fixation, immunostaining and confocal imaging.

Cell culture

Drosophila S2R+ cells were maintained at 25 °C in Schneider's Drosophila medium (Life Technologies) supplemented with 10% (v/v) FBS (Gibco) and 1% (v/v) Penicillin and Streptomycin (Invitrogen). 293T cells were maintained at 5% CO_2 in a 37 °C humidified incubator, cultured with DMEM (Invitrogen) supplemented with 10% (v/v) FBS (Gibco) and 1% (v/v) Penicillin and Streptomycin (Invitrogen). Cultured cells were transiently transfected with Effectene transfection reagent (Qiagen) according to the manufacturer's instructions.

METHOD DETAILS

Molecular biology

To generate the p10UAST-3xHA-Tace plasmid, full-length Tace was amplified by PCR from a fully sequenced cDNA clone RE65757 (Drosophila Genomics Resource Center, 18694) using the tace_NotI_fwd and the tace_XbaI_rev primer pair. The signal peptide of the *wingless* gene, plus three HA-tags, were amplified by PCR from the p10UAST-3xHA-Fra (Neuhaus-Follini and Bashaw, 2015) using the wg_AseI_fwd and the wg_EagI_rev primer pair. These two PCR products were digested with the respective restriction enzymes indicated by the names of the primers, then sequentially ligated (the wg fragment first) into a digested empty p10UASTattB vector, which contains ten UAS elements and an attB site for PhiC31-mediated targeted integration.

To generate the p10UAST-3xHA-TaceΔMP plasmid, a fragment of Tace lacking its prodomain and metalloprotease domain was amplified by PCR from RE65757 using the taceΔMP_EagI_fwd and the tace_XbaI_rev primer pair, then digested with EagI and XbaI (NEB). This fragment was then ligated into digested p10UASTattB-3xHA-Tace plasmid to generate the p10UASTattB-3xHA-TaceΔMP plasmid.

For efficient mouse spinal cord electroporation, full-length ADAM17 was subcloned from pcDNA3-ADAM17-HA (Addgene, 65105) into a pCAG vector using NotI and XhoI sites to generate pCAG-ADAM17-HA.

CRISPR Cas9-mediated mutagenesis

To generate the $tace^{CRISPR19}$ ($tace^{19}$) allele, we first cloned a plasmid containing two gRNAs targeting the first and last exons of *tace*.[73] Briefly, the tace_CRISPR_fwd and tace_CRISPR_rev primer pair, each containing homology regions flanking a 20 nucleotides (nt) long gRNA target sites, were used (IDT Inc). An insert containing the two gRNAs was amplified with this primer pair and pCFD4: U6:1-gRNA U6:3-gRNA (Addgene) as the template, digested with BbsI (NEB) then ligated back into BbsI and DpnI (NEB) digested pCFD4 backbone. Positive clones were injected by BestGene Inc. into *Drosophila* embryos that express a germline-specific Cas9 and the progeny from these flies were crossed to balancer stocks to generate stable lines. For each line, genomic DNA was extracted from two male flies and genotyped with the tace_genotyping_fwd and the tace_genotyping_rev primer pair, with an expected wild-type band of 3.3k nt and a CRIPSR KO band of 500 nt. Positive hits were confirmed by direct sequencing of these PCR fragments, which demonstrated that the entire coding sequence of *tace* is lost in the $tace^{19}$ allele (see also Figure S2A).

To generate the $tace^{CRISPR17}$ ($tace^{17}$) allele, we crossed *nos-Cas9* flies with flies that constitutively expresses a gRNA targeting the first exon of *tace*.[74] Progeny from these flies were crossed to balancer stocks to generate stable lines that do not contain the *nos-Cas9* or the gRNA transgenes. For each line, genomic DNA was extracted from two male flies and genotyped with the tace_genotyping_fwd and the tace_genotyping_rev2 primer pair. PCR products were sent for direct sequencing to identify positive hits. The $tace^{17}$ allele contains a frameshift mutation that disrupts the signal peptide sequence and generates an early stop codon in the second exon of *tace*. This ensures that even in the rare case of translation initiated by a downstream alternative start codon, the truncated Tace lacking its signal peptide should not be successfully targeted to the membrane.

Cleavage assays

Drosophila S2R+ cells plated in 6-well plates were transiently transfected with PMT-Gal4 and p10UAST expression plasmids for target proteins, using the Effectene transfection reagent (Qiagen). Cells were induced 24 hours post transfection with fresh media containing 0.5mM copper sulfate. 48 hours post transfection, medium supernatant were collected, and cells were lysed with

TBS-V buffer (150 mM NaCl, 10 mM Tris pH-8, 1 mM Sodium orthovanadate) supplemented with 0.5% Surfact-AMPS NP40 (Thermo) and 1x complete protease inhibitor (Roche) for 20 min at 4 °C with agitation. Soluble proteins in both medium supernatant and cell lysates were recovered by centrifugation at 14,000 rpm for 15 min at 4 °C. Samples were denatured by boiling at 95 °C for 10 min in 4x Laemmli SDS sample buffer (Bio-Rad) supplemented with BME (Bio-Rad) and analyzed by western blotting. Briefly, proteins were resolved by SDS-PAGE using the Mini-PROTEAN Tetra Cell system (Bio-Rad) and transferred to nitrocellulose membrane (Amersham) using the Mini Trans-Blot Module (Bio-Rad). Membranes were blocked with 5% dry milk dissolved in PBST (1x PBS supplemented with 0.1% Tween-20, Bio-rad) for one hour at room temperature and incubated with primary antibodies overnight at 4 °C with agitation. After three 5 min washes in PBST, membranes were incubated with the appropriate HRP-conjugated secondary antibodies at room temperature for one hour. After three 5 min washes in PBST, signals were detected using ECL Prime (Amersham) according to manufacturer's instructions.

HEK 293T cells plated in 6-well plates were transiently transfected with the pCMV-Dcc plasmid (gifted by Dr. Patrick Mehlen). 48 hours post transfection, cells were stimulated for 1 hour with 1 μM PMA (Sigma-Aldrich) supplemented with metalloprotease inhibitors (10 μM GM6001, 25 μM TAPI-1, 1 μM GI254023X or 10 μM GM1479) or DMSO as vehicle control. Medium supernatant and cell lysates were collected and analyzed by western blotting as described above.

Immunoprecipitation

Lysates collected from *Drosophila* S2R+ cells were pre-cleared by incubating with 30 μl of a 50% slurry of protein A and protein G agarose beads (Invitrogen) for 20 min at 4 °C with agitation. Pre-cleared lysates were recovered by centrifugation at 14,000 rpm for 15 min at 4 °C, then incubated with 1.5 μg of antibody for 30 min at 4 °C with agitation. After antibody incubation, 30 μl of a 50% slurry of protein A and protein G agarose beads (Invitrogen) was added for an additional 2 hr incubation at 4 °C with agitation. The immunocomplexes were rinsed three times with wash buffer (1XTBS supplemented with 0.1% Triton x-100 (Sigma) and 1x Complete Protease Inhibitor) and denatured by boiling at 95 °C for 10 min in 2x Laemmli SDS sample buffer (Bio-Rad) supplemented with BME (Bio-Rad) and analyzed by western blotting as described above.

To collect lysates from *Drosophila* embryos, approximately 100 μl of embryos at the desired developmental stages were treated with 50% bleach (Essendant) for 2 min and washed three times with embryo wash buffer (120 mM NaCl supplemented with 0.1% (v/v) Triton X-100, Sigma). Embryos were then rinsed with ice cold TBSV buffer (150 mM NaCl ,10 mM Tris pH 8.0, 2 mM Sodium orthovanadate), transferred to Dounce Tissue Grinders (DWK Life Sciences) and lysed in 1 ml lysis buffer (TBSV supplemented with 1% Surfact-AMPS NP40 and 1x complete protease inhibitors) by manual homogenization. Homogenized samples were then incubated for 30 min at 4 °C with agitation and recovered by centrifugation at 14,000 rpm for 15 min 4 °C. Immunoprecipitations were performed with 4 hr antibody incubation and 2 hr beads incubation. Western blotting was performed as described above.

Immunostaining

Drosophila embryos were dechorionated, formaldehyde-fixed and immunostained using standard methods.[75] Embryos were dissected and mounted in 70% (v/v) glycerol/1xPBS.

To immunostain dissociated spinal commissural neurons, first we fixed the neuron culture for 20 min at room temperature in 4% paraformaldehyde (Electron Microscopy Services), then permeabilized them for 10 min with PBT (1x PBS supplemented with 0.1% Triton X-100, Sigma) and blocked them with 2% horse serum (HS) in PBT for 30 min at room temperature.[37] Neurons were incubated with primary antibody overnight at 4 °C, secondary antibody for 1 hour at room temperature and mounted in Aquamount (Epredia).

To immunostain collagen-embedded explants, we first fixed explant cultures in 4% paraformaldehyde (Electron Microscopy Services) overnight at 4 °C, then blocked the cultures in 2.5% normal goat serum (NGS) in PBT for 2 hr at room temperature, incubated them with primary antibody overnight at 4 °C and secondary antibody overnight at 4 °C, then mounted them on cavity slides using Aquamount (Epredia).[37]

To immunostain mouse spinal cords, we first fixed E11.5 mouse embryos in 4% paraformaldehyde (Electron Microscopy Services) in PBS for 2 hr at 4 °C, then cryoprotected them in 30% sucrose overnight and frozen them in cryomolds containing Neg-50 Frozen Section Medium (Epredia) on dry ice and stored them at -80 °C.[48] Frozen embryos were sectioned to yield 20 μM transverse sections with a cryostat. Sections were blocked in 2% HS in PBT for 1h at room temperature, incubated with primary antibodies overnight at 4 °C and secondary antibodies for 2 hr at room temperature, then mounted using Aquamount (Epredia).

RNA *in situ* hybridization

RNA FISH probe for *tace* was generated by PCR amplifying the tace cDNA from RE65757 (DGRC) using the tace_NotI_fwd and the tace_insitu_rev primer pair. RNA FISH probe for *Adam17* was generated by PCR amplifying the *Adam17* sequence from pcDNA3.1-mADAM17 (Addgene) using the adam17_insitu _fwd and the Adam17_insitu_rev primer pair. The sense probe was generated in Gorla et al., 2019. For both probes, the PCR products were purified by phenol extraction and ethanol precipitation, then reverse transcribed using T7 RNA Polymerase (Promega) and DIG labeled-NTP (Roche). The reactions were terminated by DNAse (Roche) incubation, and the RNA products were precipitated by ethanol precipitation, then reconstituted in RNAse free water supplemented with an equal volume of formamide. The *comm* probe was generated as previously described.[21]

RNA FISH in *Drosophila* embryos was performed as previously described.[76] Briefly, fixed embryos underwent secondary fixation and hybridized with approximately 2 ng/μl RNA probe in hybridization buffer (50% v/v RNAse free formamide (Fisher), 1x Denhardt's

(Sigma), 500 μg/ml Salmon sperm ssDNA (Stratagene) , 250 μg/ml tRNA (Roche), 50 μg/ml heparin (Sigma), 4x SSC (Invitrogen), 0.1% Tween-20 (Bio-rad), 5% dextran sulfate (Fisher)) overnight at 4 °C. Embryos were washed for 15 min, 30 min, 45 min, 1 hr, 1 hr and 1 hr with wash buffer (50% v/v formamide (Fisher), 2x SSC (Invitrogen), 0.1% Tween-20 (Bio-Rad)) at 52°C with agitation, blocked with 5% NGS in PBT and incubated with anti-DIG-POD antibody (Roche) overnight at 4 °C. RNA FISH signals were developed by tyramide amplification using the TSA fluorescein system (AKOYA) and analyzed by confocal imaging.

RNA *in situ* hybridization in embryonic mouse spinal cord sections was performed as previously described.[77] Briefly, frozen sections were thawed, washed by PBS, underwent antigen retrieval with citric acid buffer, incubated with protease K, then acetylated with acetylation solution (0.1 M triethanolamine, 0.25% acetic anhydride). After overnight incubation with probe at 62°C, sections were then washed in 0.2X SSC at 68°C, blocked in PBT and 15% NGS at room temperature for one hour. Sections were then incubated with AP-conjugated anti-DIG antibody (Roche) in blocking buffer at 4°C overnight. After PBT washes the sections were incubated in alkaline phosphatase buffer (100 mM Tris pH9.5, 50 mM MgCl2, 100 mM NaCl, 0.1% Tween-20, 5 mM levamisole, 0.34 mg/mL NBT (Roche), 0.17 mg/mL BCIP (Roche)) for 1 hour at room temperature. Following color reaction, slides were fixed for 20 minutes in 4% PFA at room temperature, rinsed in ddH2O, dried at 37°C for 1 hour, dehydrated in xylenes and coverslipped with Aquamount (Epredia).

RNA extraction and RT-qPCR

The heads or spinal cords of E11.5 mouse embryo were fast-frozen in liquid nitrogen then stored in -80°C until ready for RNA extraction. To extract RNA from heads, the heads were mixed with 350 μl RTL buffer from RNeasy Plus Mini Kit (Qiagen), grinded with autoclaved Dounce Tissue Grinders (Wheaton) to disrupt samples, then passed 10 times through 18-gauge needles for homogenization. To extract RNA from dissected spinal cords, the spinal cords were mixed with 350 μl RTL buffer from RNeasy Mini Kit (Qiagen), then passed sequentially through 18-gauge and 20-gauge needles. After disruption and homogenization, we followed the protocol from the RNeasy Plus Mini Kit (Qiagen) to extract RNA.

cDNA was synthesized from 1μg total RNA using SuperScriptIV (Life Technologies). qRT-PCR was performed in triplicates using Fast SYBR Master Mix (Life Technologies) and analyzed on QuantStudio3 (Applied Biosystems). *Adam17* mRNA expression was quantified using the ΔΔCt method, as normalized to *Gapdh* transcript levels. Primer used in this analysis are: ADAM17_qPCR_fwd, ADAM17_qPCR_rev, GAPDH _qPCR_fwd, GAPDH _qPCR_rev.

RT-qPCR analysis using RNA extracted from E11.5 embryos detects *Adam17* transcripts in the heads or spinal cords of control embryos, which are significantly decreased in cKO embryos, further validating our cKO approach (Figures S6C and S6D). Of note, the *Nes:cre* line was reported to undergo significant germline recombination,[78] which likely contributes to the variation in *Adam17* levels in cKO embryos (Figures S6B and S6D).

Electroporation of mouse embryos and explant outgrowth assay

For each E12.5 mouse embryo, 500 ng/μl DNA was electroporated. Electroporation, dissection and culture of dorsal spinal cord explants from E12.5 mouse embryos were performed as previously described.[37] For explants cultured with Netrin-Myc transfected 293T cells, 30μg DNA was transfected 24 hours prior to plating explant cultures. Mock transfected 293T cells were used as controls. Explants were cultured for 24 hr before fixation and immunostaining as described above. For explants cultured with 500ng/ml bath applied recombinant netrin (R&D Systems), recombinant netrin was added to culturing media for 18 to 20 hr before fixation and immunostaining as described above.

Dye injections in open-book spinal cord preparations

DiI injections were performed as previously described.[48] Briefly, open-book preparations were fixed in 4% PFA for 1 hour on ice. For each open-book preparations, multiple injections were made in the dorsal edge of the spinal cord with Fast DiI (5 mg/ml, Sigma Aldrich) using a very finely pulled glass needle. Open-book preparations were then washed in cold PBS and incubated at 4°C for 3 days prior to confocal imaging.

Data and software

Confocal stacks were collected using either a spinning disk confocal system (Perkin Elmer) built on a Nikon Ti-U inverted microscope using a Nikon 40x objective (for *Drosophila* nerve cords, primary mouse neurons and mouse spinal cord sections) and a 10x objective (for mouse spinal cord sections) with the Volocity imaging software (Perkin Elmer), or a scanning confocal system built on a Zeiss LSM 800 microscope using a 20 x objective (for mouse dorsal spinal cord explants) with the Zen Lite software (Carl Zeiss). Colorimetric *in situ* hybridization images were collected using Leica DM5000B with a 10x objective and the Leica Application Suite V3 software (Leica). Images were processed using FIJI ImageJ (NIH) and Adobe Illustrator software. White balance of colorimetric *in situ* hybridization images was achieve using White balance correction_1.0 macro (Patrice Mascalchi, https://github.com/pmascalchi/ImageJ_Auto-white-balance-correction). All statistics and graphs were generated using GraphPad Prism 9.

QUANTIFICATION AND STATISTICAL ANALYSIS

For analysis of Drosophila nerve cord phenotypes, image analysis was conducted blind to genotype whenever possible. In all column scatter plots, error bars are indicated in S.E.M. For statistical analysis, statistical comparisons were made between two groups using

two-tailed Student's t-test. For multiple comparisons, significance was assessed using one-way ANOVA with Sidak tests, with family-wise alpha threshold and confidence level set at 0.05 (95% confidence interval). Chi-square test was used to assess significance in contingency table analysis. P-values are represented as follows: 0.1234 (n.s.), 0.0332 (*), 0.0021 (**), 0.0002 (***), <0.0001 (****).

For EW commissural neuron axon crossing phenotypes, filleted *Drosophila* embryos were analyzed at stages 15 and 16. Seven abdominal segments (A1 to A7) were analyzed per embryo, and for each embryo, the percentage of non-crossing segments was calculated. A segment was considered non-crossing when EW axons from at least one hemisegment failed to reach the midline, either by stalling, extending ipsilaterally or extending away from the midline. The defasciculation-like EW axon projection phenotypes were analyzed strictly at stage 16. For each embryo, the percentage of EW projection defects on either side of 14 abdominal hemisegments was calculated. EW axons were considered to have projection defects when EW axons of substantial length were protruding at the side of the main EW bundles, either ipsilaterally or away from the midline. Ectopic crossing phenotypes in FasII axon tracts or ap axons were analyzed strictly at stage 17. For each embryo, the percentage of segments with axons that ectopically crossed the midline were quantified in seven abdominal segments.

To analyze *comm* expression in stage 14 *Drosophila* embryos, we used two different approaches. First, in seven abdominal segments, we scored *comm* expression in each individual EW neuron, as determined by the presence or absence of *comm* RNA puncta in EW cell bodies. In each segment, there are six EW neurons, three per hemisegment. Thus, for each embryo, we calculated the percentage of *comm*-expressing EW neurons, which are then compared between control embryos and *tace* mutant embryos. This assay is previously described by Neuhaus-Follini and Bashaw.[1] Second, we used the average fluorescence intensity of *comm* RNA FISH in the entire nerve cord as a proxy to measure its expression level. The average fluorescence intensity of *comm* at the midline is comparable between *tace*[19] mutants and sibling control embryos (see Figure S3M), thus we used this value to normalize between images. We subtracted the *comm* RNA FISH fluorescence level at the midline from the total fluorescence level in the entire nerve cord, then normalized the value to the midline *comm* RNA FISH fluorescence level. All confocal images in this analysis were taken at the same time, with the same experimental set up.

To measure the *in vivo* Fra levels in stage 14 Fra-MIMIC-GFP *Drosophila* embryos, the SCAR-positive axon bundles were traced with the free hand tool in Image J and the mean grey values in the anti-GFP channel were normalized against those in the anti-SCAR channel. All confocal images in this analysis were taken at the same time, with the same experimental set up.

To measure the band intensities for western blots, the bands of interest were traced with the free hand tool in Image J. For each experimental condition, the mean grey value of Dcc ECD bands were normalized against the corresponding beta-tubulin bands. Three independent experiments were analyzed.

The Robo3-positive commissure thickness in transverse sections of E11.5 spinal cords were scored blind to genotype as previously described.[48] Three *Adam17* cKO animals and four *Nes:cre* negative double floxed control animals were used in our analysis. For each embryo, five to six sections at the brachial/forelimb level were quantified, then combined to obtain an averaged value. For each section, commissure thickness was normalized to the length of the spinal cord, as measured by the distance between the floor plate and the roof plate, to control for any variation in size of the embryos. Finally, the average commissure thickness of ckO embryos were normalized to sibling controls to obtain normalized commissure thickness.

To quantify the number of Brn3a or Lhx1/5 positive cells on spinal cord sections, images were first converted to black-and-white composites using the Auto-Threshold function (the default method), then counted with the Analyze Particles function in ImageJ. Three embryos were analyzed and quantified for each genotype. For each embryo, four to seven sections at the brachial/forelimb level were quantified, then combined to obtain an averaged value.

DiI injected commissural axons in open book spinal cord preparations were scored blind to genotype as previously described.[48] A total of 13 *Nes:cre* negative single or double floxed control animals (72 injection sites) and 5 cKO animals (33 injection sites) were used in our analysis. For each injection site, we quantified the percentage of axons with the phenotypes, which was then combined across all injection sites to generate a mean that was used in a Chi-square test to generate a p-value. Axons were characterized as ''normal'' when they reach the floor plate, cross the midline, and project anteriorly post-crossing. Axons that either fail to reach the floor plate or enter the floor plate but stall before crossing the midline were characterized as ''stalling before or at the midline''. Axons that either project ipsilaterally or project posteriorly post-crossing were characterized as ''abnormal turning''.

Analysis of the explant outgrowth assay cultured with cell aggregates was performed as previously described.[37] Quantification of axon outgrowth is based on beta-tubulin immunostaining signal but not RFP staining because RFP signal does not penetrate axonal processes very effectively. Explants images were converted to black-and-white composites using the Auto-Threshold function (the Li method) in ImageJ. Explants from three independent experiments were combined in our analysis. For the explant outgrowth assay cultured with 500ng/ml bath applied recombinant netrin (R&D Systems), explants images were converted to black-and-white composites using the Auto-Threshold function (the Li method) in ImageJ. For each explant, the total area of black pixels was measured for the entire circumference of the explant using the Analyze Particles function. The particles showing axonal outgrowth were then erased using the Eraser tool and the total area of black particles was measured again. The difference was recorded as total area of axonal outgrowth and normalized against the circumference of each explant. Explants harvested from three *Adam17* cKO animals and three *Nes:cre* negative double floxed control animals were used in our analysis.